

1 Seasonal provenance changes of present-day Saharan dust 2 collected on- and offshore Mauritania

3
4 Carmen A. Friese¹, Johannes A. van Hateren^{2,*}, Christoph Vogt^{1,3}, Gerhard Fischer¹, Jan-
5 Berend W. Stuut^{1,2}

6 ¹Marum-Center of Marine Environmental Sciences, University of Bremen, Bremen, 28359, Germany

7 ²NIOZ-Royal Netherlands Institute for Sea Research, Department of Ocean Systems, and Utrecht University, 1790
8 AB, Den Burg Texel, Netherlands

9 ³ZEKAM, Crystallography, Geosciences, University of Bremen, 28359, Germany

10 *Now at: Vrije Universiteit Amsterdam, Faculty of Earth Sciences, 1081 HV Amsterdam, the Netherlands

11 *Correspondence to:* Carmen A. Friese (cfriese@marum.de)

12 **Abstract.**

13 Saharan dust has a crucial influence on the earth climate system and its emission, transport, and deposition are
14 intimately related to e.g. wind speed, precipitation, temperature and vegetation cover. The alteration in the physical
15 and chemical properties of Saharan dust due to environmental changes is often used to reconstruct the climate of
16 the past. However, to better interpret possible climate changes the dust source regions need to be known. By
17 analysing the mineralogical composition of transported or deposited dust, potential dust source areas can be
18 inferred. Summer dust transport offshore Northwest Africa occurs in the Saharan air layer (SAL). In continental
19 dust source areas dust is also transported in the SAL, however the predominant dust input occurs from nearby dust
20 sources with the low-level trade winds. Hence, the source regions and related mineralogical tracers differ with
21 season and sampling location. To test this, dust collected in traps onshore and in oceanic sediment traps offshore
22 Mauritania during 2013 to 2015 was analysed. Meteorological data, particle-size distributions, back-trajectory and
23 mineralogical analyses were compared to derive the dust provenance and dispersal. For the onshore dust samples,
24 the source regions varied according to the seasonal changes in trade-wind direction. Gibbsite and dolomite
25 indicated a Western Saharan and local source during summer, while chlorite, serpentine and rutile indicated a
26 source in Mauritania and Mali during winter. In contrast, for the samples that were collected offshore, dust sources
27 varied according to the seasonal change in the dust transporting air layer. In summer, dust was transported in the
28 SAL from Mauritania, Mali and Libya as indicated by ferrylglauconite and zeolite. In winter, dust was transported
29 with the Trades from Western Sahara as indicated by e.g. fluellite.

31 **Keywords**

32 Saharan dust, MWAC, sediment trap, mineralogy, particle size, major potential source area, provenance

33 1 Introduction

34 Mineral dust influences global climate through many feedback mechanisms and is in turn influenced by variations
35 in environmental parameters. The emission, transport and deposition of mineral dust reacts sensitively to
36 parameters of climate change like rainfall, wind, temperature and vegetation cover (Knippertz and Stuut, 2014).
37 In turn, the emission, transport and deposition of mineral dust has an impact on the atmospheric energy balance
38 (Haywood and Boucher, 2000), precipitation distribution and amplitude (Yoshioka et al., 2007), sea surface
39 temperatures (Lau and Kim, 2007) as well as the oceanic carbon pump (Martin et al., 1991; Martin, 1990; Jickells
40 et al., 2005; Iversen et al., 2010; Iversen and Robert, 2015; Ploug et al., 2008a). The sensitivity of mineral dust to
41 environmental parameters is used to reconstruct the climate of the past (Rea, 1994; Tjallingii et al., 2008; Mulitza
42 et al., 2010; Diester-Haass and Chamley, 1978; Holz et al., 2007; Stein, 1985). For instance, the particle size of
43 mineral dust in ocean sediment records varies according to the paleo-frequency of dust-storm and rainfall events
44 (e.g., Friese et al. (2016)). Further, the mineralogical composition of mineral dust in sediment core records can be
45 used as a qualitative proxy for paleo-dust source activity (Scheuven et al., 2013).

46 Every year, about 2000Mt dust are emitted from source areas around the world, of which 75% are deposited on
47 land and 25% into the oceans (Shao et al., 2011). The Saharan Desert is the world's largest source of mineral
48 aerosols with an annual dust transport of ~180 Mt westwards towards the North Atlantic (Yu et al., 2015). About
49 140Mt is actually deposited into the North Atlantic Ocean (Yu et al., 2015). Therefore, Saharan mineral dust
50 constitutes an essential component of the global climate system. The source regions of Saharan dust have been
51 studied frequently by analysing the mineralogical composition of dust collected at continental sites
52 (e.g. Skonieczny et al. (2013); Skonieczny et al. (2011); Schütz and Sebert (1987); Kandler et al. (2009); Khiri et al.
53 (2004)), during aircraft flights (e.g. Formenti et al. (2008)), on research ships (Chester et al., 1971; Chester et al.,
54 1972; Stuut et al., 2005; Aston et al., 1973; Chester and Johnson, 1971b; Chester and Johnson, 1971a) and with
55 gravity cores offshore NW Africa (Biscaye, 1964; Biscaye, 1965; Lange, 1982; Rateev et al., 1969; Griffin et al.,
56 1968; Diester-Haass and Chamley, 1978; Meyer et al., 2013). Continental dust studies in northern Morocco revealed
57 that dust is produced predominantly locally (Khiri et al., 2004; Kandler et al., 2009). For instance, a high percentage
58 of quartz and feldspar and a low amount of micas in the dust samples was interpreted to represent mostly local
59 dust sources and the availability of calcite sources from proximal coastal dunes in Morocco (Khiri et al., 2004).
60 Further, also in Morocco, dust was sampled in Tinfou at a height of 4 m during the SAMUM 2006 field campaign.
61 These samples were analysed for their physical and chemical properties. The particle size correlated to local
62 surface wind speed suggesting the contribution of local dust (Kandler et al., 2009). In contrast, in coastal Senegal
63 dust is sourced by the Sahel during winter as shown by low illite/kaolinite (I/K) ratios and lower palygorskite
64 contents as opposed to the summer samples which were suggested to be originating from the Sahara (Skonieczny
65 et al., 2013). Further, the I/K ratio in dust sampled on the Cape Verde Islands showed that dust was derived from
66 strongly varying sources: north-western Sahara, central and southern Sahara and the Sahel (Caquineau et al.,
67 2002). The results of the above mentioned studies imply that dust collected on land is predominantly of local
68 provenance, while the sources of dust sampled offshore NW Africa are of regional and long-distance provenance.
69 As a result, a large seasonal difference can be expected in the composition of the marine climate archives, related
70 to the different dominating transport mechanisms of dust in summer and winter (Friese et al., 2016).

71 To test this, we compared the mineralogical composition, the fluxes, and the particle size of Saharan dust sampled
72 from 2013-2015 in Iwik (Mauritania) in on-land dust traps with Saharan dust sampled from 2013-2015 offshore
73 Cape Blanc (Mauritania) in sub-marine sediment traps and with the scientific dust-collecting buoy 'Carmen'. By
74 comparing the data with meteorological data, back trajectories, the African lithology and satellite images we aim
75 to address the following questions:

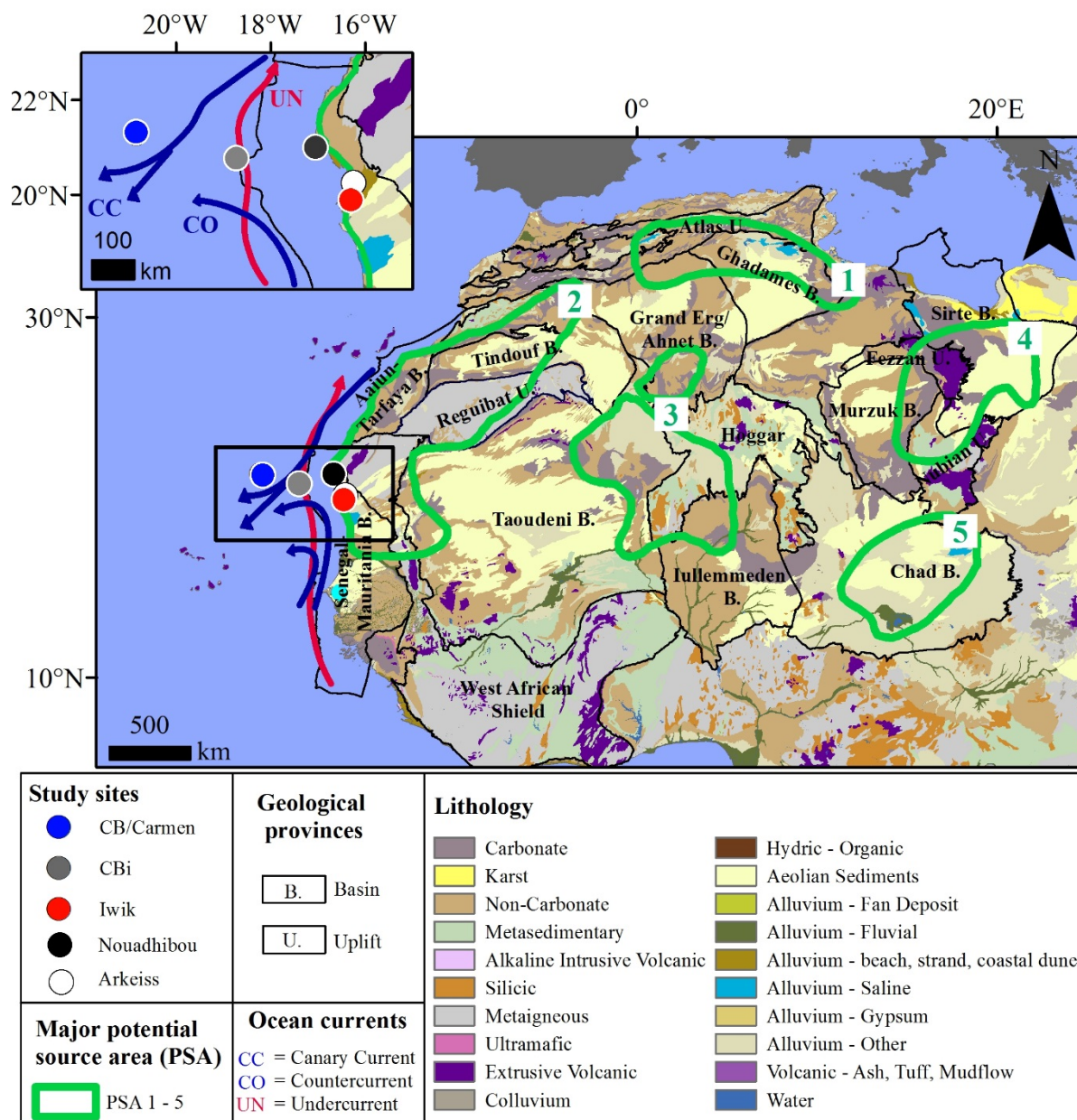
- 76 1) What is the seasonal variability in the particle size of mineral dust deposited on land? How does the
77 variability relate to meteorological parameters (wind speed, precipitation)?
- 78 2) What are the source regions of dust trapped on land versus dust trapped in the ocean?
- 79 3) Can we identify characteristic minerals that constitute a tracer for certain source areas?

80 **1.1 Study sites and North African dust sources**

81 In Fig. 1 the location of the study sites and North African dust sources are displayed. The dust-collecting buoy
82 'Carmen' (~21°15' N, ~20°56' W) and the sediment trap mooring site CB (~21°16' N, ~20°48' W) are virtually
83 at the same position ~ 200 nautical miles offshore Cape Blanc. Sediment-trap station CBi (~20°45' N, ~18°42' W)
84 is located ~ 80 nautical miles offshore Cape Blanc. The continental dust collector Iwik (~ 19°53' N, ~ 16°18' W)
85 and the meteorological station Arkeiss (~ 20°7' N, ~ 16°15' W) are located in a major potential dust source area
86 (**PSA 2**) in the Parc National de Banc d'Arguin (PNBA) near Iwik and near Arkeiss in Mauritania. A further
87 meteorological station is positioned in the **PSA 2** in Nouadhibou (~ 20°55' N, ~ 17°1' W) in the Western Sahara.

88
89 The major PSA of northern African dust are summarized in a review by Scheuven et al. (2013). Predominant
90 dust transport towards western Africa and offshore the Atlantic Ocean occurs from the foothills of the Atlas
91 mountains, Western Sahara and Western Mauritania (**PSA 2**), southern Algeria and northern Mali (**PSA 3**) and
92 Western Chad including the Bodélé depression (**PSA 5**) (Scheuven et al., 2013). In contrast, dust sourced from
93 Tunisia and northern Algeria (**PSA 1**) is transported predominantly to the western Mediterranean and Western
94 Europe (Stuut et al., 2009). Central Libya (**PSA 4**) is the most important region for dust transport to the eastern
95 Mediterranean (Scheuven et al., 2013).

96



97

98 **Figure 1: Map of the study sites under investigation: the scientific buoy Carmen as well as the sediment trap moorings**
 99 **CB and CBi offshore Cape Blanc, the MWAC dust collector onshore near Iwik and the surface station near Nouadhibou**
 100 **and Arkeiss(shapefile of the surface lithology and the geological provinces: downloaded from the USGS website**
 101 **<http://rmgsc.cr.usgs.gov/ecosystems/africa.shtml#SL> and**
 102 **<http://certmapper.cr.usgs.gov/geoportal/catalog/main/home.page>, major potential dust source areas: redrawn from**
 103 **Scheuvens et al. (2013), ocean currents: redrawn from Mittelstaedt (1991)).**

104 1.2 Geological characterisation of dust-producing areas

105 In the following, the lithology of the geological provinces that underlay the major PSA's is outlined (Fig. 1).

106 The **PSA 1** is underlain by the eastern Atlas chain and the northern Grand erg/Ahnet and Ghadames Basins. The
 107 outcrops in the Atlas uplift are composed of e.g. limestones, sandstones and evaporites (Piqué, 2001). The thick
 108 strata overlying the northern Ahnet and Ghadames Basin consist of e.g. sandstones and mudstones (Selley, 1997b).

109 The **PSA 2** is underlain by the Reguibat Shield, the Mauritanides and the Senegal-Mauritania, Aaiun-Tarfaya,
110 Tindouf and Taoudeni Basins. The western part of the Reguibat Shield is dominated by granitic rocks, while the
111 eastern part is dominated by metamorphic and granitic rocks (Schofield et al. (2006) and references therein). West
112 of the Reguibat Shield, the Mauritanides consist of a metamorphic belt and ophiolite (Villeneuve, 2005). West of
113 the Taoudeni Basin, the Mauritanides are characterized by granites, quartzites and strongly metamorphosed rocks
114 (Villeneuve, 2005). While the Aaiun-Tarfaya Basin features outcrops with dolomites and limestones, the Senegal-
115 Mauritania Basin is characterized by very few carbonate deposits (Bosse and Gwosdz, 1996). The Tindouf Basin
116 is characterized by mainly sandy deposits (Selley, 1997c, b). The local soils surrounding the dust collector site
117 Iwik are composed of sandy deposits often rich in fossil shells and partly cemented by lime (Einsele et al., 1974).

118 The **PSA 3** is underlain by the western Hoggar and parts of the Ahnet, Taoudeni and Iullemeden Basins. The
119 Pharusian belt located in the western Hoggar is characterized by Eburnean granulites, gneiss, graywackes and
120 magmatic rocks (Boullier, 1991). In the southern Ahnet Basin sandstone strata crop out. On the eastern edge of
121 the Taoudeni Basin outcropping sediments are characterized by conglomerates, sandstones and limestones
122 (Bertrand-Sarfati et al., 1991). The outcrops of the Iullemeden Basin are composed of e.g. sandstones,
123 carbonaceous shale, laterites and massive clays (Kogbe, 1973).

124 The **PSA 4** is underlain by parts of the Fezzan and Nubian uplifts and the Sirte and Murzuk Basins. The eastern
125 Fezzan uplift consists of ocean island basalts (Cvetković et al., 2010; Abdel-Karim et al., 2013), while sediments
126 outcropping in the northern Nubian uplift are composed of e.g. sandstones, limestones and gypsiferous horizons
127 (El Makkrouf, 1988). The southern Sirte Basin is covered by sands, gravel and sand seas (Selley, 1997a). Outcrops
128 of the eastern Murzuk Basin are composed of marine limestones and alluvial sandstones (Selley, 1997b, c).

129 The **PSA 5** is underlain by the Chad Basin. During the Holocene, the Chad Basin was filled with fine-grained
130 particles from the drainage of the Tibesti mountains to the north (Prospero et al., 2002). Hence, the sediments that
131 outcrop in the central Chad Basin are characterized by fluvial and alluvial sediments such as laminated diatomites,
132 pelites and coastal sandridges (Schuster et al., 2009).

133

134 **1.3 Atmospheric setting**

135 Saharan dust emission, transport and deposition are related to seasonal variations in atmospheric circulation
136 (Knippertz and Todd, 2012). The intertropical convergence zone (ITCZ) shifts meridionally from ~12 °N during
137 boreal winter to ~21 °N during boreal summer resulting in a seasonal change in rainfall and winds over the African
138 continent (Nicholson, 2009).

139 During summer, continental rainfall is most intense and the rain belt is positioned near ~10°N with smaller amounts
140 of rainfall near ~21°N. Dust emission is driven by low level jets, ‘haboobs’, African easterly waves (AEWs) and
141 high surface winds associated with the Saharan heat low (Knippertz and Todd, 2012). Low-level N trade winds
142 blow and transport dust in coastal Mauritania year-round (National Geospatial-Intelligence Agency, 2006).
143 Saharan dust is transported on- and offshore within the ‘Saharan air layer’ (SAL) at an altitude of about 3 km
144 (Diaz et al., 1976; Carlson and Prospero, 1972; Prospero and Carlson, 1972; Prospero and Carlson, 1970).

145 During winter, dust emission is driven by the break-down of nocturnal low-level jets after sunrise, increased surges
146 in Harmattan winds and microscale dust devils and dust plumes (Knippertz and Todd, 2012; Koch and Renno,
147 2005). Dust is transported within the low-level NE and E trade winds to coastal Mauritania (Dobson, 1781) and
148 also offshore to the sediment-trap mooring sites (Stuut et al., 2005).

149 **1.4 Oceanic setting**

150 The surface-water circulation offshore Cape Blanc is influenced by the southward-flowing Canary Current (CC)
151 and the poleward-flowing coastal counter current or Mauritania Current (Fig. 1). Underneath, the undercurrent is
152 flowing poleward in water depths down to 1000 m (Fig. 1). The undercurrent flows along the continental slope
153 and transports water masses originating from ~5-10 °N to latitudes up to 26 °N. The poleward flowing South
154 Atlantic Central Water (SACW) and the southward flowing North Atlantic Central Water (NACW) are situated
155 below the counter current and meet offshore Cape Blanc (Mittelstaedt, 1991). The study area is positioned in a
156 zone of permanent annual upwelling of sub-surface water masses (Cropper et al., 2014). The NACW and SACW
157 may be upwelled and mixed laterally off Cape Blanc (Meunier et al., 2012). The permanent annual upwelling of
158 nutrient-rich subsurface waters results in high phytoplankton concentrations offshore Cape Blanc (Van Camp et
159 al., 1991). As a result, the surface waters are rich in organic detritus, usually referred to as ‘marine snow’, and
160 faecal pellets which are produced by marine zooplankton (Iversen et al., 2010).

161

162 Individual Saharan dust particles which settle at the ocean surface hardly settle to the deep sea. Instead, fine dust
163 particles can be transferred from the ocean surface to the deep sea by being incorporated into marine snow
164 aggregates and faecal pellets (Ternon et al., 2010). The aggregate formation and ballasting of marine snow
165 aggregates and faecal pellets with marine carbonate and opal as well as with Saharan dust particles results in
166 anomalously high sinking velocities (Iversen and Robert, 2015; Fischer and Karakas, 2009; Iversen and Ploug,
167 2010; Iversen et al., 2010; Ploug et al., 2008b). Dust-loaded particles that sink into the deeper water column are
168 assumed to have a mean settling speed of ~ 240 m d⁻¹ at site CB (Fischer and Karakas, 2009).

169

170

171

172

173

174

175

176

177

178

179

180

181

182

183

184

185 **2. Material and Methods**

186

187 In Table 1 an overview of the material and methods employed for each study site is presented. Bulk sediment
 188 samples were obtained at the sites CB and CBi and dust samples at the sites Carmen and Iwik. All samples were
 189 analyzed for particle size and dust flux with the exception of the site Carmen, of which only dust particle size was
 190 analyzed. Only the sites CBi and Iwik were analyzed for mineral assemblages and only the samples of the site
 191 Iwik were used for microscopic investigation. Meteorological sensors were available for the stations Carmen, Iwik
 192 and Arkeiss, while for the site Nouadhibou meteorological data was downloaded online. TRMM precipitation data
 193 was downloaded online for all sites except for the site Nouadhibou.

194

195 **Table 1: Overview of the material and methods employed at each study site.**

Study site	Lat./lon.	Samples	Analysis	Meteorological sensor and data	Downloaded meteorological data
Carmen	~21°15' N, ~20°56' W	1 MWAC sample	particle size	Vaisala WXT520: wind direction + speed, precipitation	TRMM 3B42: precipitation
CB	~21°16' N, ~20°48' W	38 sediment trap samples	lithogenic fluxes, particle size	-	TRMM 3B42: precipitation
CBi	~20°45' N, ~18°42' W	38 sediment trap samples	lithogenic fluxes, particle size, mineral assemblages	-	TRMM 3B42: precipitation, HYSPLIT back trajectories
Iwik	~19°53' N, ~16° 18' W	24 MWAC samples	microscopy, dust fluxes, particle size, mineral assemblages	Davis 6250 Vantage Vue: wind direction + speed	TRMM 3B42: precipitation, HYSPLIT back trajectories
Nouadhibou	20° 55' N, 17° 1' W	-	-	-	Wind direction + speed
Arkeiss	~20° 7' N, ~16° 15' W	-	-	Davis 6250 Vantage Vue: precipitation	TRMM 3B42: precipitation

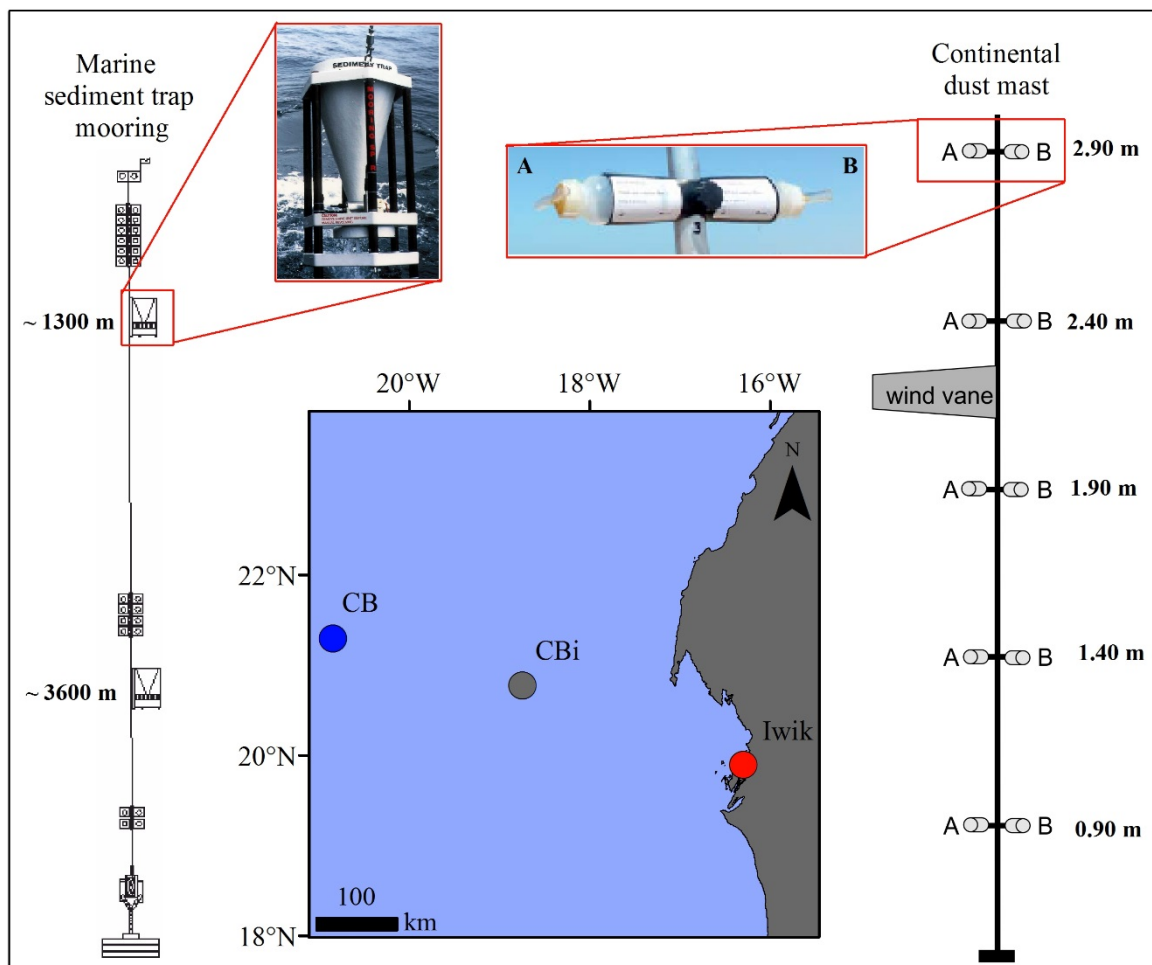
196

197 **2.1 Sediment traps**

198

199 Saharan dust was collected in the ocean using marine sediment traps of the type Kiel (model SMT-234/243) which
 200 are conical with an opening of 0.5 m² (Fig. 2). The principle of particle collection is much the same as described
 201 by Van der Does et al. (2016) and Korte et al. (2017). At the top of the opening a honeycomb grid is installed to

202 prevent large swimmers (>1 cm) from entering the trap. The sediment traps were equipped with twenty sample
 203 cups which rotated according to a pre-programmed sampling interval (Fischer and Wefer, 1991). The sampling
 204 interval was chosen depending on the timing of the ship expeditions.



205
 206 **Figure 2: The marine sediment trap moorings CB and CBi offshore Cape Blanc and the dust masts near Iwik,**
 207 **Mauritania. On the left, a sketch of the sediment trap mooring (sketch of CB 24 copied from Fischer et al. (2013))**
 208 **together with a photograph of the trap (downloaded from www.kum-kiel.de) is displayed. On the right, a sketch of the**
 209 **dust mast together with a photograph of the MWAC sampling bottles is depicted.**

210
 211 The sampling intervals were synchronized between the two sites. The intervals ranged from 9.5 days to 21.5 days
 212 (Table 2). Deployment and recovery of the sediment-trap samples was performed during the Research Vessel
 213 Poseidon expeditions POS445 (Fischer et al., 2013), POS464 (Fischer et al., 2014) and POS481 (Fischer et al.,
 214 2015a) (Table 2). The working steps related to the trap deployment and treatment are described in Fischer and
 215 Wefer (1991). In order to prevent outflow of water from the cups during sampling, each sampling cup was filled
 216 with 20 ml of filtered (<0.2 μm) seawater with a salinity of 40 ‰. To produce seawater with a salinity of 40 ‰,
 217 100 g NaCl suprapur was added to 1 l of filtered seawater. Microbial and zooplankton activity was inhibited inside
 218 the trap samples by adding 1 ml of a saturated solution of the biocide HgCl₂ per 100 ml of seawater. After recovery,
 219 swimmers <1 cm were removed from the samples by sieving each sample through a 1 mm mesh. A McLane rotary
 220 liquid splitter was used to split the <1 mm fraction of each sample into five equal aliquots.
 221 The samples of two sediment-trap deployments during 2013–2015 of the sediment trap mooring stations CB and
 222 CBi were chosen for grain-size analyses (Table 2). The upper traps sampled at an average water depth of ~ 1300

223 m and the lower trap sampled at a water depth of ~3600 m (Table 2). Dust which settles at the ocean surface is
 224 advected by ocean currents during settling in the water column. As a result, particles that settle in an area of ~ 40
 225 x 40 km² in the ocean surface above the traps may be collected in a water depth of ~ 1300 m (Friese et al., 2016).
 226 Two winter and two summer samples were chosen for X-ray Diffraction (XRD) measurements (Table 3).

227 **Table 2: Specifications of the sediment trap samples collected during 2013-2015 chosen for flux and grain-size analysis.**

Trap series	Trap type	Sampling period	Cruise deployment	Cruise recovery	Position	Trap depth [m]	Water depth [m]	No. of samples	Sampling intervals
CBi 11 upper (GeoB 18006-2)	SMT 243	29.01.2013 – 25.03.2014	Pos445	Pos464	20°46.4' N 18°44.4' W	1406	2800	18	17x21d, 1x20d
CBi 12 upper (GeoB 19402-01)	SMT 234 NE	14.02.2014 - 23.02.2015	Pos464	Pos481	20°46.4' N 18°44.5' W	1356	2750	20	1x12.5 d, 19x19.5
CB 24 upper (GeoB 18001-1)	SMT 234 NE	24.01.2013 - 05.02.2014	Pos445	Pos464	21°16.9' N 20°50.6' W	1214	4160	18	1x26 d, 16x21 d, 1x15 d
CB 25 lower (GeoB 19401-1)	SMT 234 NE	07.02.2014 – 21.02.2015	Pos464	Pos481	21°17.8' N 20°47.8' W	3622	4160	20	19x19.5 d, 1x9.5 d

228

229 **Table 3: Sediment trap and MWAC samples chosen for mineralogical investigation.**

Sample	Sampling period	Mast	Bottle	Elevation/water depth [m]	Sampling interval
CBi 11 upper # 8	25.06.-16.07.13	-	-	1406	21d
CBi 12 upper # 2	26.02.-18.03.14	-	-	1356	20d
CBi 12 upper # 10	01.08.-21.08.14	-	-	1356	20d
CBi 12 upper # 17	16.12.-04.01.15	-	-	1356	19d
Iwik 13-7-2-3B	24.06.-15.07.13	2	B	1.90	21d
Iwik 14-8-2-5B	15.08.-15.09.14	2	B	2.90	31d
Iwik 14-12-1-4A	15.12.14-18.01.15	1	A	2.40	34d
Iwik 14-2-2-5B	15.02.-15.03.14	2	B	2.90	28d

230

231

232 2.2 Modified Wilson and Cooke (MWAC) samplers

233 Saharan dust was collected on land near Iwik, Mauritania, with a passive dust sampler consisting of two masts (1
 234 and 2) with two sets of five air sampling bottles each (A and B, Fig. 2). The dust sampling bottles are referred to
 235 as modified Wilson and Cooke (MWAC) samplers (Mendez et al., 2011; Wilson and Cooke, 1980) and consist of
 236 a closed Polyethylene bottle through which the wind can pass via two glass tubes of 8 mm openings. Thus, a big
 237 difference between the traps and the MWAC collectors is the much smaller collection area of the MWAC collectors

238 with 44 mm². The MWAC dust sampler was chosen because it is one of the most common (Zobeck et al., 2003)
 239 and most efficient dust samplers (Goossens and Offer, 2000). The sampling bottles were mounted horizontally at
 240 five different heights.

241 The samples collected in 2013-2015 were chosen for subsequent flux and grain-size analyses (Table 4). Saltating
 242 dust particles may be collected in the lower sampling bottles at 90 cm. However, the aim was to analyse dust
 243 transported in suspension to enable a better comparison between the continental and marine sites. Therefore, the
 244 highest sampling bottles attached to the mast at 2.90 m height were used for microscope, flux and grain-size
 245 analysis (Table 3). One series of bottles (series B2) of mast 2 were analysed with the microscope. The other three
 246 replicate samples (bottles A1 and B1 of mast 1, bottles A2 of mast 2) were analysed for flux and grain-size analysis.
 247 Out of the three replicate samples, the sample with the highest mass was chosen for the interpretation of the flux
 248 and grain-size data because this bottle was assumed to have sampled most efficiently. Three samples mounted at
 249 a height of 2.40 m of mast 2 were chosen to test the effect of the chemical pre-treatments that we do to isolate the
 250 terrigenous fraction from marine sediments on the resulting grain-size distributions (Fig. 2). Two winter and two
 251 summer samples that contained enough material were chosen for XRD measurements (Table 3).

252 Furthermore, dust was sampled with a MWAC dust sampler mounted on the mast of buoy Carmen, at about 2 m
 253 above the sea surface (Stuut et al., 2015). The masts of the buoy ‘Carmen’ and of the Iwik dust sampler were
 254 aligned to the ambient wind direction via a wind vane (Fig. 2). This MWAC dust sample was also analysed for
 255 grain-size distribution.

256 **Table 4: Specifications of the MWAC samples collected during 2013-2015 chosen for flux and grain-size analysis.**

Dust collector series	Trap type	Sampling period	Position	Height [m]	No. of samples	Sampling intervals
Iwik 13	MWAC	27.01.2013 – 20.01.2014	19°53.1' N 16° 17.6' W	2.90	11	19 d, 28 d, 32 d, 29 d, 40 d, 21 d, 31 d, 61 d, 31 d, 31 d, 35 d
Iwik 14	MWAC	20.01.2014 - 18.01.2015	19°53.1' N 16° 17.6' W	2.90	13	26 d, 28 d, 31 d, 30 d, 31 d, 30 d, 31 d, 31 d, 30 d, 32 d, 29 d, 34 d
CB-MWAC	MWAC	23.08.2014 – 16.11.2015	21°15.8' N 20°56.1' W	2.00	1	450 d

257

258 2.3 Microscopy

259 The MWAC samples chosen for microscopic investigation were analysed with a Leica M165 C microscope.
 260 Microscope pictures were taken using a Leica DFC420 camera attached to the microscope. The software Leica
 261 application suite 3.8 was used for taking the pictures.

262

263 2.4 Dust and lithogenic fluxes

264 1/5 splits of the sediment trap samples were analysed for dust fluxes and the bulk components following the method
 265 presented in Fischer and Wefer (1991). The lithogenic flux [mgm⁻²d⁻¹] was estimated according to Eq. (1):

$$266 \quad \textit{lithogenic material} = \textit{dust} = \textit{total mass} - \textit{carbonate} - \textit{opal} - 2 \times \textit{Corg} \quad (1)$$

267 Organic carbon was measured after the removal of carbonate with 2N HCl using a CHN-Analyser (HERAEUS).
268 Total carbon was estimated by combustion without pre-treatment. Carbonate was determined according to Eq. (2):

$$269 \quad \text{carbonate} = \text{total carbon} - \text{organic carbon} \quad (2)$$

270 Biogenic opal was determined with a sequential leaching technique (Müller and Schneider, 1993).
271 The MWAC samples chosen for dust flux analyses were weighed on a Mettler-Toledo AT261 Delta Range balance
272 with a precision of 0.0001 g. Mean atmospheric dust concentrations were estimated as Eq. (3):

$$273 \quad DL = \frac{MAR}{(v \cdot A)} * \frac{1}{\eta} \quad (3)$$

274 where DL is the mean dust concentration [μgm^{-3}], MAR is the mass accumulation rate [μgs^{-1}], v is the mean wind
275 speed per sampling month [ms^{-1}], A is the cross-sectional area of the inlet tube of the MWAC sampler [m^2] and η
276 is the estimated sampling efficiency of MWAC bottles. A sampling efficiency of 90 % was assumed based on an
277 efficiency study of Goossens and Offer (2000). Mean horizontal dust fluxes were calculated according to Eq. (4):

$$278 \quad F_h = \frac{MAR}{A} * \frac{1}{\eta} \quad (4)$$

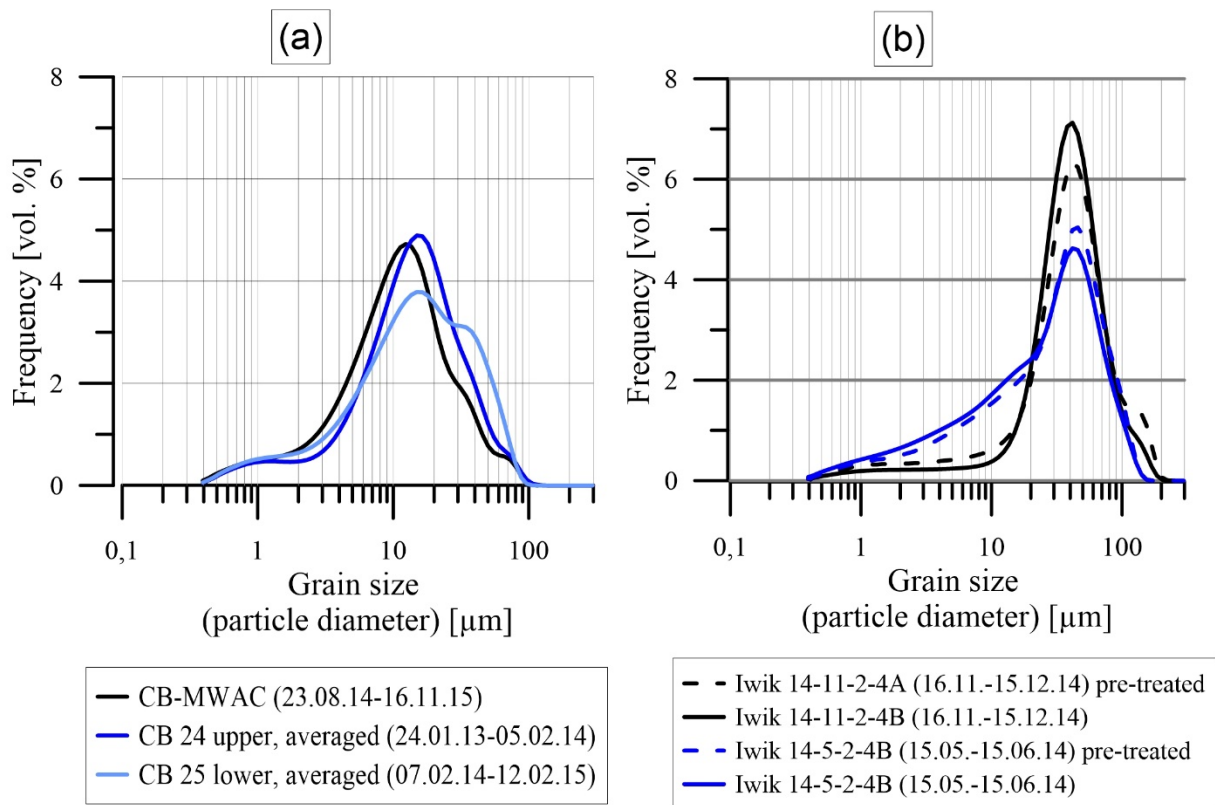
279 where F_h is the horizontal dust flux [$\text{mgm}^{-2}\text{d}^{-1}$], MAR is the mass accumulation rate [mgd^{-1}], A is the cross-
280 sectional area of the inlet tube of the MWAC sampler [m^2] and η is the estimated sampling efficiency of MWAC
281 bottles.

282 **2.5 Particle size**

283 A 1/25 split of the marine sediment trap samples was analysed for particle size of the terrigenous fraction. The
284 samples were pre-treated before measurement in order to isolate this fraction (see also Filipsson et al. (2011); Friese
285 et al. (2016), Meyer et al. (2013) and Stuut (2001) for methodology) with the following steps: (1) removal of
286 organic matter: Addition of 10 ml of H_2O_2 (35%) to the sediment sample and subsequent boiling until the reaction
287 stops, (2) removal of calcium carbonate: Addition of 10 ml HCl (10%) to the sediment sample and subsequent
288 boiling for exactly 1 minute and (3) removal of biogenic silica: Adding 6 g of NaOH pellets to the sediment sample
289 and subsequent boiling for 10 minutes. Before particle-size analysis, 10 drops of $\text{Na}_4\text{P}_2\text{O}_7 \cdot 10\text{H}_2\text{O}$ were added to
290 each sample to assure the full disaggregation of the particles. The pre-treatment of the MWAC samples differed
291 from the pre-treatment of the sediment trap samples as, obviously, these samples did not contain any biogenic
292 material originating from marine plankton. Further, the disaggregation of particles needed to be kept at minimum
293 to allow for the study of dust transport processes, the so-called 'minimally dispersed' aeolian fraction (McTainsh
294 et al., 1997). Therefore, the MWAC samples were solely pre-treated with three drops of $\text{Na}_4\text{P}_2\text{O}_7 \cdot 10\text{H}_2\text{O}$ before
295 analysis. The marine sediment-trap samples as well as the MWAC samples were analysed with the laser particle
296 sizer Beckmann Coulter LS13320 at NIOZ using a Micro Liquid Module (MLM). This instrument allows quick,
297 accurate, and precise data acquisition of large size intervals (Bloemsma et al., 2012). An analytical error of ± 1.26
298 μm ($\pm 4.00\%$) was considered for the measurements (Friese et al., 2016).

299 To investigate the comparability of the MWAC samples with the oceanic sediment-trap samples, the particle-size
300 distribution of the MWAC sample attached to buoy Carmen was compared to the averaged particle-size
301 distributions of the upper and lower trap series at site CB (Fig. 3a). The grain-size distribution of the MWAC
302 sample was comparable to both sediment trap time series even though the sampling time period was different. To

303 ensure that the pre-treatment steps of the traps did not influence the terrigenous fraction itself, tests were made in
 304 which the on-land MWAC samples were exposed to the same pre-treatment steps as the marine samples (Fig. 3b).
 305 One spring sample has been measured with and without a chemical pre-treatment. Two fall dust samples were
 306 obtained from the same height and mast and sampling interval, however from different bottles (A and B) and were
 307 measured with and without pre-treatment. The figure indicates that a pre-treatment of the Iwik dust samples did
 308 not alter the particle distributions of the samples significantly. Further, the particle-size distribution of dust sampled
 309 with different bottles is comparable.



310

311 **Figure 3: (a) Grain-size distributions for the station CB: Dust sampled with the MWAC sampler 2 m above sea level,**
 312 **with the upper sediment trap at 1214 mbsl and the lower trap at 3622 mbsl. (b) Grain-size distributions of samples of**
 313 **the Iwik 14 time series which have been pre-treated with HCl, H₂O₂ and NaOH (dotted lines) and without pre-**
 314 **treatment (lines).**

315 2.5 Mineral assemblages

316 Two winter and two summer samples of the MWAC dust collector and the sediment-trap series CBi were chosen
 317 for XRD analysis (Table 4). X-Ray Diffraction pattern analyses were carried out in the laboratory of the research
 318 group Crystallography (University of Bremen, Central Laboratory for Crystallography and Applied Material
 319 Sciences, ZEKAM, Dept. of Geosciences).

320 Due to the small amount of material in the available dust samples (< 100 mg), the preparation for the measurement
 321 was done by pipetting a demi-water-sample mixture on glass slides. A thorough preparation commonly increases
 322 reproducibility of the results, however, the standard deviation given by Moore and Reynolds (1989) of ±5% can
 323 be considered as a general guideline for mineral groups with >20% clay fraction. In addition, the determination of
 324 well-crystallized minerals like quartz, calcite or aragonite can be done with better standard deviations (Tucker and

325 Tucker, 1988; Vogt et al., 2002). The X-Ray Diffraction was measured on a Philips X'Pert Pro multipurpose
326 diffractometer equipped with a Cu-tube ($k\alpha$ 1.541, 45 kV, 40 mA), a fixed divergence slit of $\frac{1}{4}^\circ$, a secondary Ni-
327 Filter and the X'Celerator detector system. The measurements were carried out as a continuous scan from $3 - 85^\circ$
328 2θ , with a calculated step size of $0.016^\circ 2\theta$ (calculated time per step was 100 seconds). Mineral identification was
329 accomplished using the Philips software X'Pert HighScore™, which, besides the mineral identification, can give
330 a semi-quantitative value for each identified mineral on the basis of Relative Intensity Ratio (R.I.R.)-values. The
331 R.I.R.-values are calculated as the ratio of the intensity of the most intense reflex of a specific mineral phase to the
332 intensity of the most intense reflex of pure corundum (I/I_c) referring to the “matrix-flushing method” after Chung
333 (1974). Unfortunately R.I.R. values are sparse for clay minerals and long chain organic materials hampered the
334 quantification of our samples.

335 **2.6 Meteorological data**

336 The obtained flux and size data were compared to near-by meteorological data (wind speed, wind direction and
337 precipitation).

338 Wind direction, wind speed and precipitation data with a 20 minute resolution were gathered for the sampling site
339 CB ($21^\circ 17' N - 21^\circ 12' N$, $20^\circ 56' W - 20^\circ 54' W$) during the buoy Carmen deployments from November 2013 to
340 September 2015 with a Vaisala WXT520 meteorology sensor. The size of the dataset was reduced by calculating
341 four hour averages. Moreover, wind direction and wind-speed data with a resolution of five minutes to one hour
342 were gathered during sampling at site Iwik ($19^\circ 53.1' N$, $16^\circ 17.6' W$) from January 2013 to January 2015 with a
343 Davis 6250 Vantage Vue meteorology sensor. The size of the dataset was reduced by calculating one-hour
344 averages. Further hourly precipitation data were gathered from the station Arkeiss ($20^\circ 7' N$, $-16^\circ 15' W$) from
345 December 2013 to March 2015 with another Davis 6250 Vantage Vue meteorology sensor. Continental hourly
346 wind direction and wind-speed data was acquired for the Nouadhibou meteorological station ($20^\circ 55' N$, $17^\circ 1'$
347 W) online from the Cedar Lake Ventures website (<https://weatherspark.com>).

348 Local daily precipitation data (TRMM 3B42 dataset, 0.25° spatial resolution) were derived from the Giovanni
349 online data system, developed and maintained by the NASA GES DISC (<http://gdata1.sci.gsfc.nasa.gov>). Daily
350 precipitation data were downloaded as area-averages around CBI ($20^\circ 58' N - 20^\circ 34' N$, $18^\circ 56' W - 18^\circ 32' W$),
351 Iwik ($19^\circ 41' N - 20^\circ 5' N$, $16^\circ 29' W - 16^\circ 05' W$), CB/Carmen ($21^\circ 05' N - 21^\circ 29' N$, $21^\circ 02' W - 20^\circ 38' W$) and
352 Arkeiss ($20^\circ 19' N - 19^\circ 55' N$, $16^\circ 28' W - 16^\circ 04' W$) according to the assumed catchment area of the upper trap
353 ($\sim 40 \times 40 \text{ km}^2$).

354 Maps of six hourly mean surface wind vectors and speed (20th century reanalysis V2c dataset) were provided by
355 the NOAA/OAR/ESRL PSD (Boulder, Colorado, USA) and downloaded from their website
356 (<http://www.esrl.noaa.gov/psd/>). **2.7 Mapping with ArcMap**

357 The mapping software ArcMap version 10.3.1 was used to analyze the source regions of the dust samples
358 investigated for mineralogical composition. A map was created with four-day back-trajectories for days with a
359 dust-storm event as depicted on satellite images. In addition, the African surface lithology was included in the map
360 and soils rich in the minerals calcite, kaolinite and chlorite were marked.

361 Satellite quasi-true colour RGB images (MODIS dataset) were retrieved from the NASA Worldview website
362 (<https://worldview.earthdata.nasa.gov>).

363 Four-day back trajectories at altitudes of 10 m (following Stuu et al. (2005)), 100 m, 3000 m, 4500 m (following
364 Skonieczny et al. (2013)) and 5500m were calculated ending at the dust collector site Iwik (19°52' N, 16°17' W)
365 and at the proximal marine trap site CBi (20°46',18°44' W) using the Hybrid Single Particle Lagrangian
366 Integrated Trajectory (HYSPLIT) model (Stein et al., 2015) and the reanalysis dataset (2.5° spatial resolution) on
367 the NOAA website (<http://ready.arl.noaa.gov>).

368 An ArcGIS layer file of the African surface lithology
369 (new_af_lithology_w_glbvtr_waterbdy_90m_dd84_final.lyr) was downloaded from the U.S. Geological survey
370 (USGS) website (<http://rmgsc.cr.usgs.gov>).

371 An ArcGIS shape file of the African soils (DSMW.shp) was downloaded from the website of the food and
372 agriculture organization of the United Nations (FAO) (<http://www.fao.org>). The mean percentages of calcite
373 (8.9 %), chlorite (4.1 %) and kaolinite (29 %) in the clay fraction of Saharan soils in general and for each soil type
374 is given by Journet et al. (2014). Soils with larger percentages of calcite, chlorite or kaolinite in the clay fraction
375 than the average percentages were marked in the ArcGIS map.

376

377

378

379

380

381

382

383

384

385

386

387

388

389

390

391

392

393

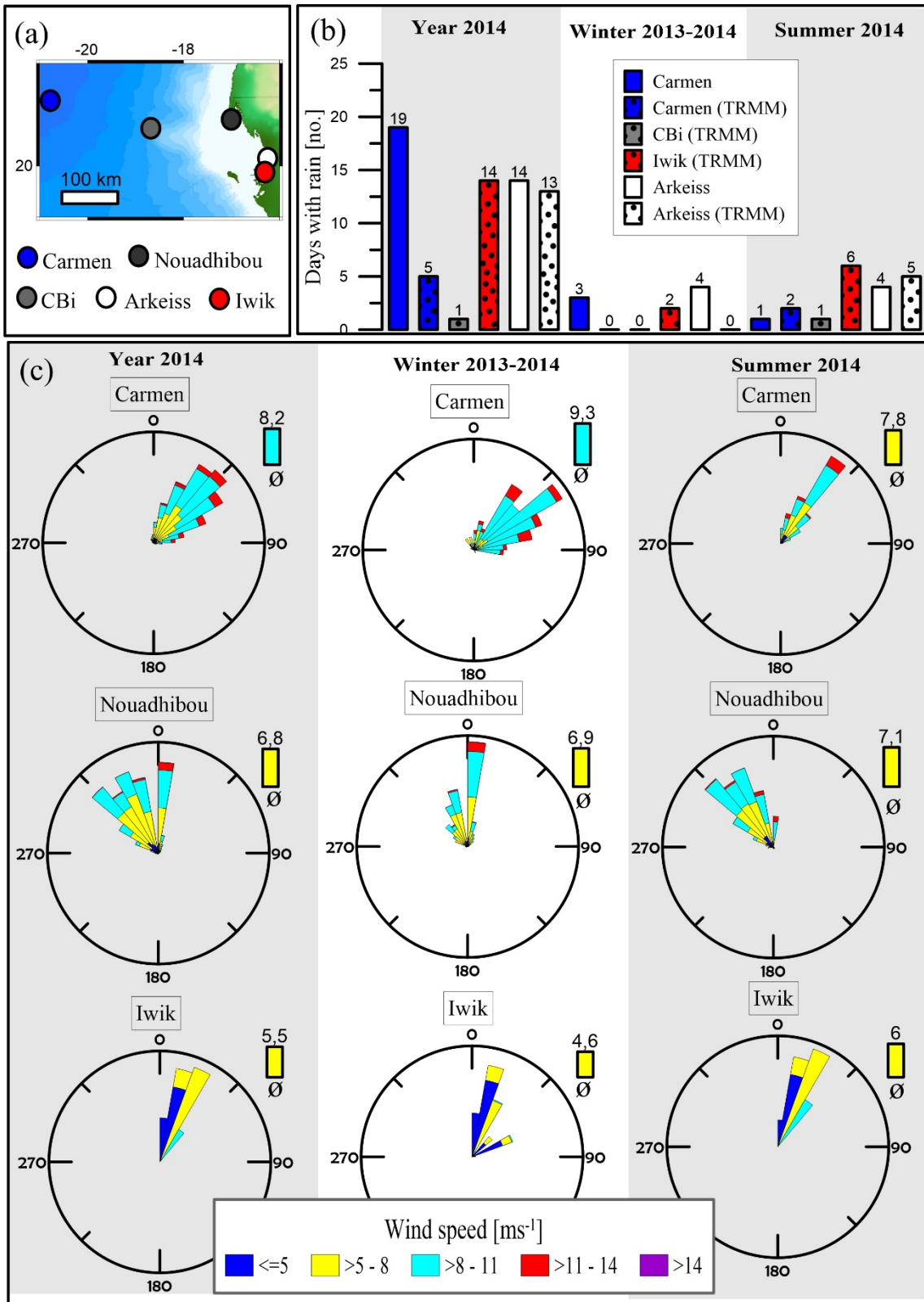
394 **3. Results**

395 **3.1 Meteorology**

396 In Fig. 4 the meteorological data of the sites Carmen (CB), CBI, Iwik, Arkeiss and Nouadhibou during 2013 to
397 2014 are presented (see Fig 4a for location of the sites). The rainfall frequency is given in Fig. 4b for each site.
398 The number of rainfall events were calculated regarding the TRMM stations for precipitation rates $>1 \text{ mmd}^{-1}$
399 because smaller precipitation amounts which were detected by the satellite may not actually reach the ground.
400 Regarding the surface stations Carmen and Arkeiss, a threshold of $>0.2 \text{ mmd}^{-1}$ was used in order to exclude events
401 which may be related to anomalously high moisture instead of rainfall.

402 According to the TRMM satellite product the annual precipitation frequency was larger on the shoreline (station
403 Arkeiss and Iwik) than offshore (station CBI and Carmen) (Fig. 4b). This may be explained by a decrease in
404 atmospheric water vapor content due to precipitation when the winds move westward. Moreover, the TRMM
405 satellite product indicated larger rainfall frequencies during the summer season compared to the winter season
406 regarding the stations Carmen, CBI, Iwik and Arkeiss. Larger summer rainfall frequencies can be explained by the
407 summer northward shift of the ITCZ to $\sim 21^\circ \text{ N}$ resulting in more frequent moist convection and rainfall in the
408 study area.

409 The annual rainfall frequency at the site Arkeiss and the summer rainfall frequencies at the sites Arkeiss and
410 Carmen compare quite well between the sensors and the TRMM observations. However, the spatial and seasonal
411 trends observed by the TRMM data were not supported by the sensor on buoy Carmen and by the surface station
412 in Arkeiss. The larger annual and winter rainfall frequency recorded with the sensor on buoy Carmen may be
413 related to water emission from the ocean surface during time periods with strong surface winds. Further,
414 disagreements between the surface stations and the TRMM stations may be caused by the local signal recorded by
415 the respective rain sensor. A larger number of rain sensors would most likely improve the comparability to the
416 TRMM data.



417

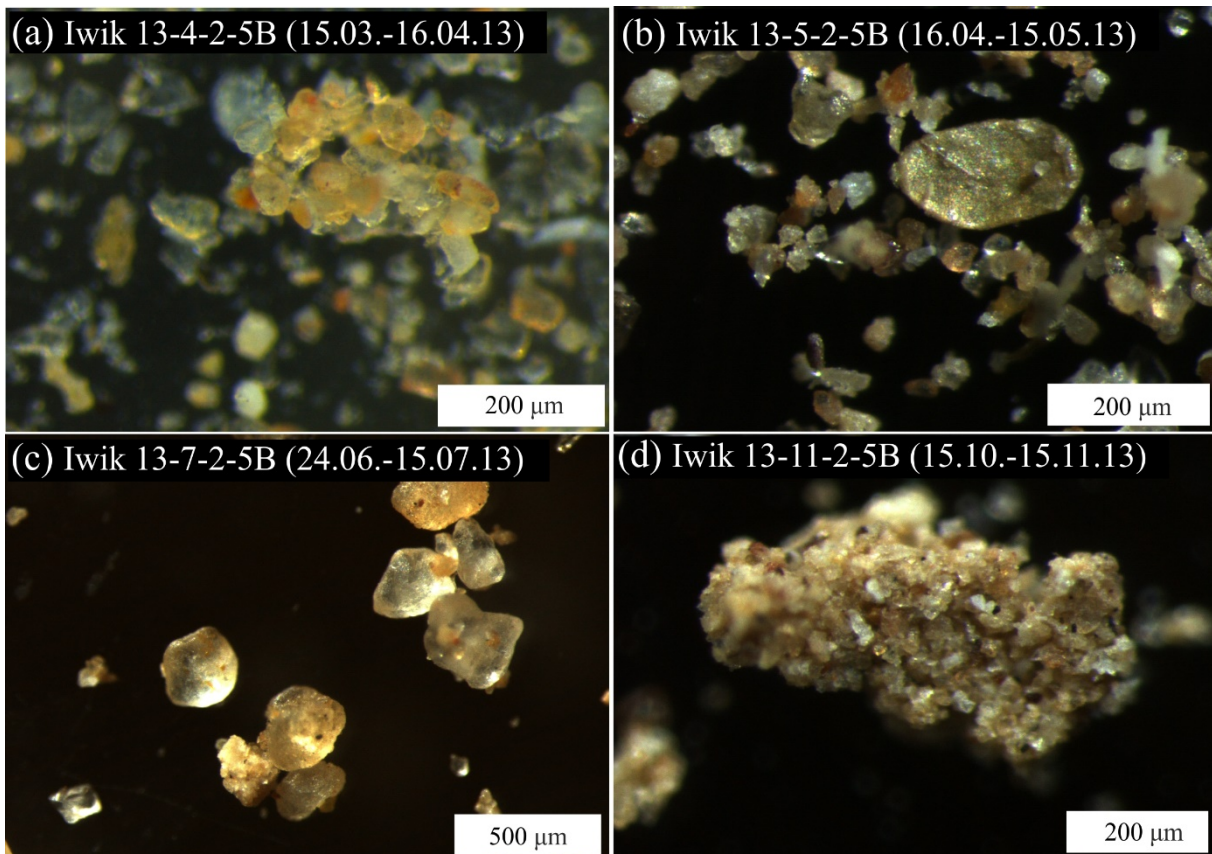
418 **Figure 4: Meteorological data (a) map showing the sites Carmen (CB), CBi, Iwik, Nouadhibou and Arkeiss under**
 419 **investigation (b) precipitation at the sites Carmen(CB), CBi, Iwik and Arkeiss (c) wind direction and speed at the**
 420 **sites Carmen (CB), Nouadhibou and Iwik.**

421 The wind direction and speed for the surface stations Carmen, Nouadhibou and Iwik are displayed in Fig. 4c. The
 422 annual average surface wind velocity was maximum offshore at buoy site Carmen(CB) with $\sim 8 \text{ ms}^{-1}$. The buoy

423 recorded a larger average wind velocity during winter than during summer, which is consistent with this season
424 being dominated by the Trades. On the shoreline, the average wind velocity was slightly larger during summer
425 than during winter. The predominant annual wind direction was NE at site Carmen and Iwik, while predominant
426 NW winds were recorded for the site Nouadhibou. The wind direction changed from predominant NE during
427 winter to predominant NNE direction during summer at site Carmen. A similar, but less pronounced seasonal trend
428 can be observed for the continental site Iwik. In Nouadhibou, the predominant winter wind direction is NNW
429 switching to a predominant NW wind direction during summer. Obviously, with winds originating from the open
430 ocean, not a lot of dust is anticipated. Therefore, we interpret these wind directions as being very local and caused
431 by the shape of the peninsula of Cape Blanc.

432 3. 2 Microscope findings of the dust samples from Iwik

433 In Fig. 5 the results of the microscopy investigation of the Iwik 2013 time series are presented. In general, the
434 majority of the particles consisted of angular and moderately spherical quartz grains with a diameter of $\sim 50 \mu\text{m}$
435 (Fig. 5a,b). A small percentage of large platy minerals with a diameter of $\sim 200 \mu\text{m}$ were found in all samples (Fig.
436 5b). Large quartz grains with a diameter of ~ 150 to $200 \mu\text{m}$ were detected in 45 % of the samples. An anomalously
437 high percentage of sub-angular and moderately spherical quartz grains with an average diameter of $\sim 200 \mu\text{m}$ was
438 observed in one summer sample (Fig. 5c). Aggregated grains occurred in all samples. However, the percentage
439 and size of the aggregates as well as the size of the aggregated grains differed from sample to sample. Usually, the
440 size of the aggregated grains was $\sim 50 \mu\text{m}$ (Fig. 5a). Two samples were characterized by aggregates composed of
441 particles with a smaller size of $\sim 20 \mu\text{m}$ (Fig. 5d).



442

443 **Figure 5: Microscopic photographs of selected dust samples from the Iwik 2013 time series. (a) Spring dust sample with**
 444 **a ~ 250 x 150 µm aggregate, (b) spring dust sample with a ~ 200 x 100 µm mica chip, (c) summer dust sample with ~**
 445 **200 x 200 µm quartz grains, (d) fall dust sample with a ~ 600 x 250 µm aggregate.**

446 **3.3 Dust fluxes and size on land and in the ocean**

447 In Table 5 the average dust fluxes are given for the sampling sites Iwik, CBi and CB. The dust concentrations at
 448 site Iwik were determined based on the measured wind speed of the meteorological sensor attached to the sampling
 449 mast. For four samples no wind data were available due to a failure of the instrument. For these samples a wind
 450 velocity was assumed based on the seasonal averages calculated from the available wind data of the meteorology
 451 sensor in Iwik (Fig. 4c). The annual average horizontal dust fluxes at site Iwik were of the same order of magnitude
 452 during 2013 and 2014. The annual average dust fluxes decreased from the on-land site Iwik towards the proximal
 453 site CBi and the distal site CB. At site Iwik the average dust concentration was maximum during spring plus
 454 winter 2013 and 2014 with 393 µgm⁻³ and 341 µgm⁻³, respectively, and minimum in fall 2013 and 2014 with 48
 455 and 68 µgm⁻³, respectively. The dust fluxes generally decreased with collection height in the mast between 90 and
 456 290 cm (not shown).

457 **Table 5: Seasonal and annual average dust fluxes and average modal grain size, mean/mode ratio and standard**
 458 **deviation of the grain-size distributions from Iwik 13-14, CBi 11-12 upper and CB 24 upper time-series.**

Series	Year	Winter	Summer	Annual
<i>Average dust fluxes [mg.m⁻².d⁻¹] (dust concentration [µg.m⁻³])</i>				
Iwik 13	2013	10000 (30)	113000 (268)	95000 (214)
CBi 11 upper	2013	106	168	99
CB 24 upper	2013	53	44	45
Iwik 14	2014	208000 (603)	55000 (127)	102000 (275)
CBi 11+12 upper	2014	98	20	47
<i>Average modal grain size [µm]</i>				
Iwik 13	2013	44	49	48
CBi 11 upper	2013	27	39	29
CB 24 upper	2013	16	17	16
Iwik 14	2014	45	49	48
CBi 11+12 upper	2014	34	44	33
<i>PM₁₀ [vol. %]</i>				
Iwik 13	2013	13	18	17
CBi 11 upper	2013	31	38	34
CB 24 upper	2013	34	31	34
Iwik 14	2014	13	27	19
CBi 11+12 upper	2014	30	37	31
<i>Average mean/mode ratio [µm]</i>				
Iwik 13	2013	0.7	0.6	0.6
CBi 11 upper	2013	0.5	0.3	0.5
CB 24 upper	2013	0.7	0.8	0.7
Iwik 14	2014	0.6	0.4	0.6
CBi 11+12 upper	2014	0.5	0.3	0.5
<i>Average standard deviation [µm]</i>				
Iwik 13	2013	2.8	3.1	3.0
CBi 11 upper	2013	3.0	3.3	3.1
CB 24 upper	2013	2.7	2.6	2.6
Iwik 14	2014	2.8	3.5	3.1
CBi 11+12 upper	2014	3.1	3.3	3.0

459

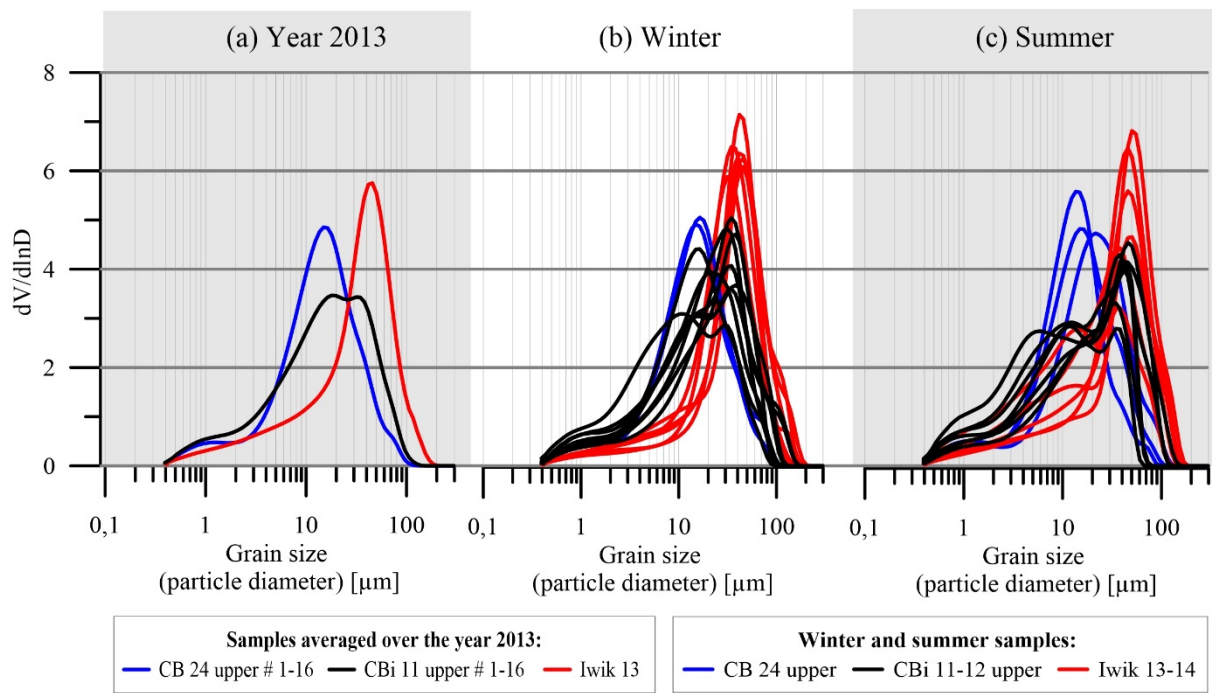
460 The statistical values of the measured grain-size distributions for the stations CB, CBI and Iwik are given in Table
461 5. In addition, the measured grain-size distributions for the time series of the stations CB, CBI and Iwik are
462 displayed in Fig. 6. In Fig. 6a the average grain-size distribution for the samples of each of the three stations for
463 the year 2013 are given. The maximum measured particle size decreased from $\sim 223 \mu\text{m}$ on land at site Iwik to
464 $\sim 169 \mu\text{m}$ at the proximal site CBI and $\sim 140 \mu\text{m}$ at the distal site CB (Fig. 6a). In addition, the average modal grain
465 size decreased from $\sim 48 \mu\text{m}$ at site Iwik to $16 \mu\text{m}$ at site CB (Table 5). Bimodal grain-size distributions were
466 encountered for 23 % of the CBI 11-12 samples, 13 % of the Iwik 13-14 samples, and none of the CB 24 samples.
467 The three bimodal distributions of the Iwik 13-14 time series were characterized by an additional smaller coarse
468 mode population peaking at $\sim 16 \mu\text{m}$ besides the more pronounced and variable larger coarse mode population
469 peaking at ~ 42 to $55 \mu\text{m}$. The three Iwik dust samples characterized by a smaller coarse mode population were
470 collected during spring, summer (Fig. 6c) and fall. The eight bimodal grain-size distributions of the CBI 11-12
471 time-series were characterized by a variable larger coarse mode population at ~ 25 to $35 \mu\text{m}$ and a variable smaller
472 coarse mode population at ~ 6 to $16 \mu\text{m}$. The bimodal distributions were recorded for three winter, three summer
473 (Fig. 6b,c), one spring and one fall sample. The annual average PM_{10} percentage is about two times larger at the
474 offshore sampling sites CB and CBI compared to the onshore sampling site Iwik. On average, about one third of
475 the dust mass sampled at the sites CB and CBI is composed of particles smaller than $10 \mu\text{m}$. The average geometric
476 standard deviation was smaller of the CB samples with $2.6 \mu\text{m}$ compared to the Iwik and CBI time series with 3.1
477 μm (Table 5). The lowest average mean/mode ratio was recorded for the CBI time-series with ~ 0.5 (Table 5).

478 In Fig. 6b-c the measured grain-size distributions for winter and summer samples are displayed. The averaged
479 modal grain size for the summer samples was coarser grained compared to the winter samples of the respective
480 grain-size time series (Table 5). The seasonality in modal grain size was largest for the CBI 11 upper trap series
481 of the year 2013 with a difference of $\sim 12 \mu\text{m}$ (Table 5). On average, the PM_{10} percentage was larger for dust
482 sampled during summer compared to winter at the sites Iwik and CBI. An opposite, however less pronounced,
483 seasonal trend could be observed for the site CB with generally larger PM_{10} percentages during winter compared
484 to summer. The average standard deviation was larger and the average mean/mode ratio was smaller in the summer
485 samples compared to the winter samples regarding the sites Iwik and CBI (Table 5). This seasonal trend was not
486 observed in the CB 24 upper samples . (Table 5).

487

488

489



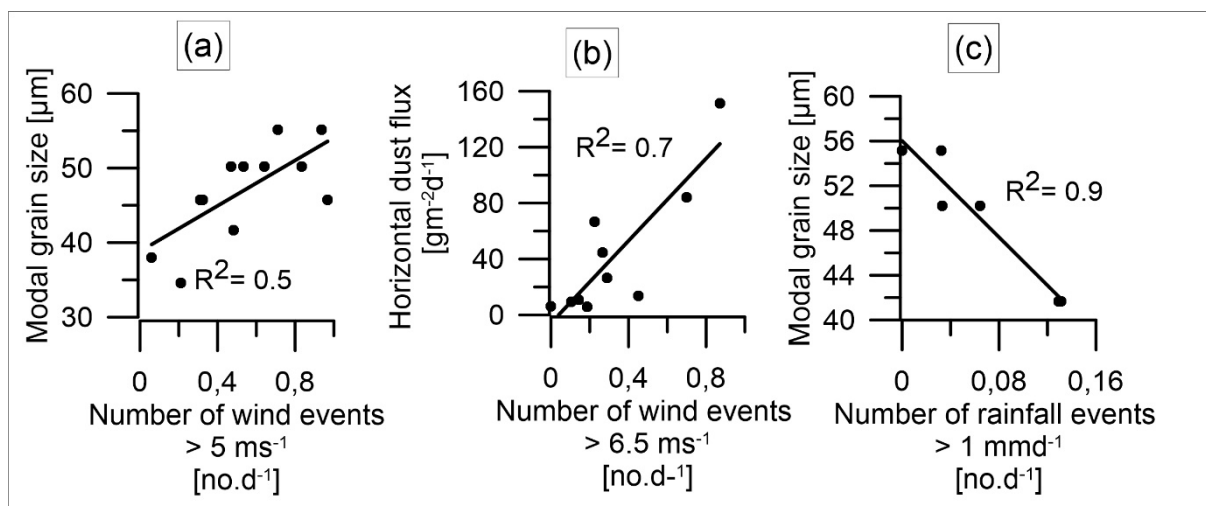
490

491 **Figure 6: Grain-size distributions of the stations Iwik, CBI and CB (a) averaged for the samples of the year 2013 (b)**
 492 **winter samples (c) summer samples.**

493 In Fig. 7a –c the results of the correlation between the characteristics of the dust sampled on land and the local
 494 meteorological data are presented. In Fig. 7a the particle sizes were correlated to the surface wind speed data (N =
 495 13 samples). A correlation above a coefficient of determination (R^2) of 0.3 was considered significant at the 95 %
 496 confidence level for two-tailed probabilities. The modal particle size of the Iwik samples showed a positive linear
 497 correlation with the daily wind speed events with $R^2 = 0.5$, which is significant at the 99.31 % confidence level.
 498 The correlation was only evident when using a threshold for wind events of 3.5 to 5.5 ms^{-1} and was best for a
 499 threshold of 5 ms^{-1} . A better positive linear correlation was obtained when excluding the spring sample resulting
 500 in $R^2 = 0.7$ which is significant at the 99.96 % confidence level.

501 In Fig. 7b the dust fluxes were correlated to the surface wind-speed data (N = 10 samples). A correlation above R^2
 502 = 0.4 was considered significant at the 95 % confidence level for two-tailed probabilities. The horizontal dust flux
 503 of the Iwik samples correlated positively to the daily wind speed events during the sampling interval with $R^2 = 0.7$
 504 which is significant at the 99.75 % confidence level. The correlation was only evident when using a threshold for
 505 wind events of 6.5 to 7 ms^{-1} and was best for a threshold of 6.5 ms^{-1} . Moreover, a significant linear correlation
 506 with $R^2 = 0.6$ was observed at the 99.15 % confidence level between the dust fluxes and the mean wind strengths
 507 during the sampling intervals (not shown).

508 In Fig. 7c the particle size of the Iwik summer samples was correlated to the local TRMM precipitation data (N= 6
 509 samples). In this case a correlation above $R^2 = 0.7$ was considered significant at the 95 % confidence level for two-
 510 tailed probabilities. A good linear negative correlation with $R^2 = 0.9$ was observed which is significant at the 99.78
 511 % confidence level.



512

513 **Figure 7: Correlation between the observed local surface wind speed at site Iwik and the measured (a) modal grain size**
 514 **and (b) flux. (c) Correlation between the observed local precipitation at site Iwik (TRMM data) and the modal grain**
 515 **size of the summer samples.**

516 **3.4 Mineral assemblage of dust sampled on land and in the ocean**

517 In Table 6 the mineralogical composition averaged over all eight samples, averaged over the four Iwik samples
 518 and the four CBI samples is given. All dust samples contained the minerals quartz and mica. Further minerals that
 519 occurred with significant quantities but which were not present in all dust samples were feldspar, amphibole,
 520 zeolite, chlorite and palygorskite. Calcite, dolomite, gibbsite, kaolinite, smectite, sepiolite, fluellite, anhydrite,
 521 rutile and serpentine occurred only in some samples resulting in a low average abundance $\leq 1\%$. However, we
 522 argue that these minerals can be used as dust source indicators because of (1) the characteristic distribution of
 523 gibbsite, kaolinite, smectite and sepiolite in North Africa according to different weathering regimes (Biscaye,
 524 1964) and (2) the characteristic occurrence of fluellite, anhydrite, rutile and serpentine according to outcropping
 525 rock type (Deer et al., 1992). Further minerals that occur in low abundances ($\leq 3\%$) were summarized as ‘other
 526 minerals’ and will not be discussed in the manuscript. While the continental samples were dominated by quartz
 527 and feldspar, the marine samples were dominated by mica, followed by quartz and feldspar.

528 **Table 6: Results of the mineralogical investigation: Mineral assemblage averaged over all samples (Total), the Iwik**
 529 **samples (Iwik) and the CBI samples (CBI).**

*	Qz [%]	Fsp [%]	Mi [%]	Amf [%]	Pal [%]	Chl [%]	Cc [%]	Dol [%]	Gib [%]	Zeo [%]	Kao [%]	Sme [%]	Se [%]	Rut [%]	Serp [%]	Ga [%]	Anh [%]	Flu [%]
Total	25.1	21.5	25.5	5.1	3.4	4.4	0.6	0.1	1.0	3.8	0.9	0.4	1.1	0.5	0.3	0.1	0.1	1.1
Iwik	33.3	30.8	18.0	5.0	3.3	1.8	1.3	0.3	2.0	0.0	0.0	0.0	0.0	0.8	0.5	0.0	0.0	0.0
CBI	17.0	12.3	33.0	5.3	3.5	7.0	0.0	0.0	0.0	7.5	1.8	0.8	2.3	0.3	0.0	0.3	0.3	2.3

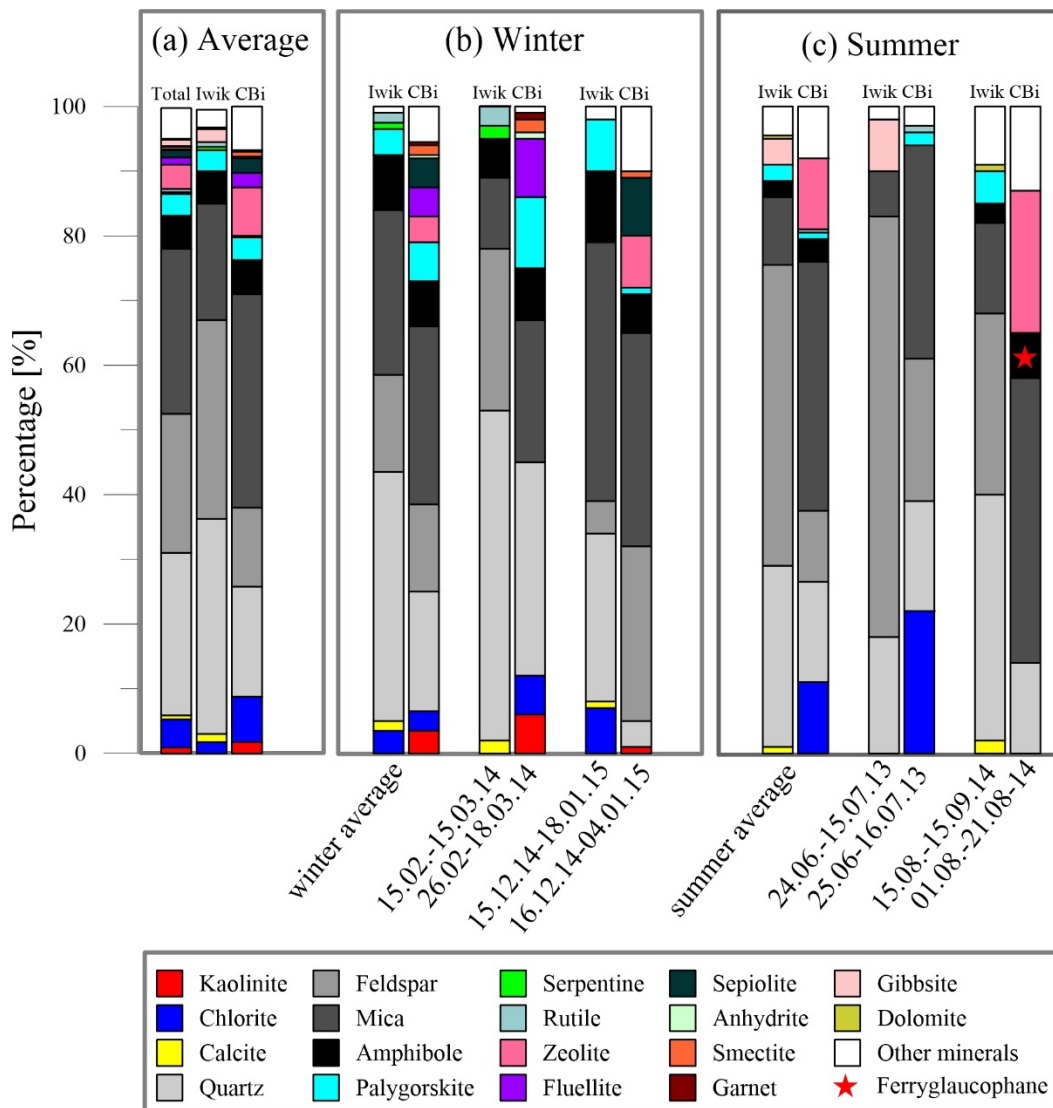
*Qz = quartz, Fsp = feldspar, Mi = mica, Amf = amphibole, Pal = palygorskite, Chl = chlorite, Cc = calcite, Dol = dolomite, Gib = gibbsite, Zeo = zeolite, Kao = kaolinite, Sme = smectite, Se = sepiolite, Rut = rutile, Serp = serpentine, Ga = garnet, Anh = anhydrite, Flu = fluellite

530

531 In Fig. 8a-c the results of the mineralogical investigation of the eight chosen dust samples are presented. Figure 8a
 532 depicts again the average composition of the samples per sampling site (N=4). The minerals zeolite, anhydrite,
 533 garnet, sepiolite, fluellite, kaolinite and smectite were only found in the marine samples. Only the continental
 534 sample of 15.08.-15.09.14 contained traces of zeolite. While gibbsite, serpentine, calcite and dolomite were
 535 detected in the continental dust samples, these minerals were absent in all marine samples. The absence of calcite

536 and gibbsite may have been caused by the pre-treatment of the marine sediment-trap samples with HCl. Although
 537 the concentration of the used acid is fairly low (10%) and the exposure time of the samples was exactly 1 minute,
 538 we cannot exclude that carbonate minerals were dissolved. Therefore, the absence of these minerals in the marine
 539 traps will not be discussed further.

540 In the following, the seasonality in the average mineralogical composition will be outlined for each site as given
 541 in Fig. 8b,c. At site Iwik, the winter dust samples were characterized by the occurrence of chlorite, serpentine and
 542 rutile, while the summer samples were characterized by the minerals gibbsite and dolomite. At site CBI, the winter
 543 dust samples were characterized by the occurrence of the minerals sepiolite, fluellite, kaolinite, smectite, garnet
 544 and anhydrite, while the summer samples were characterized by the mineral rutile. Only for the marine trap
 545 samples an annual average chlorite/kaolinite ratio (C/K = 4) could be derived owing to the occurrence of kaolinite.



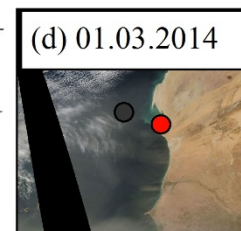
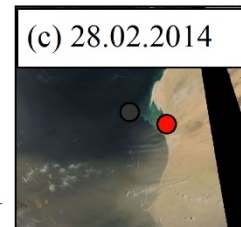
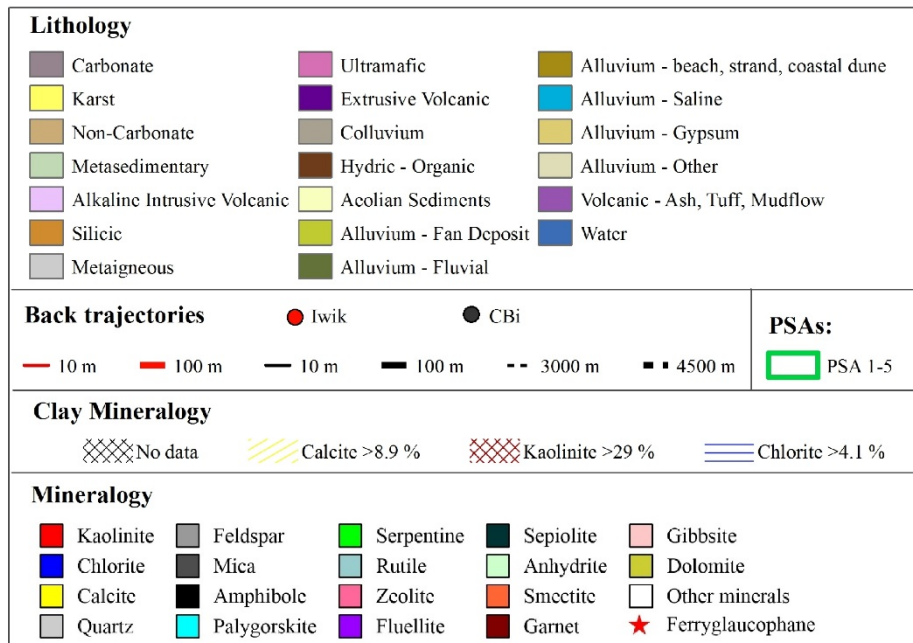
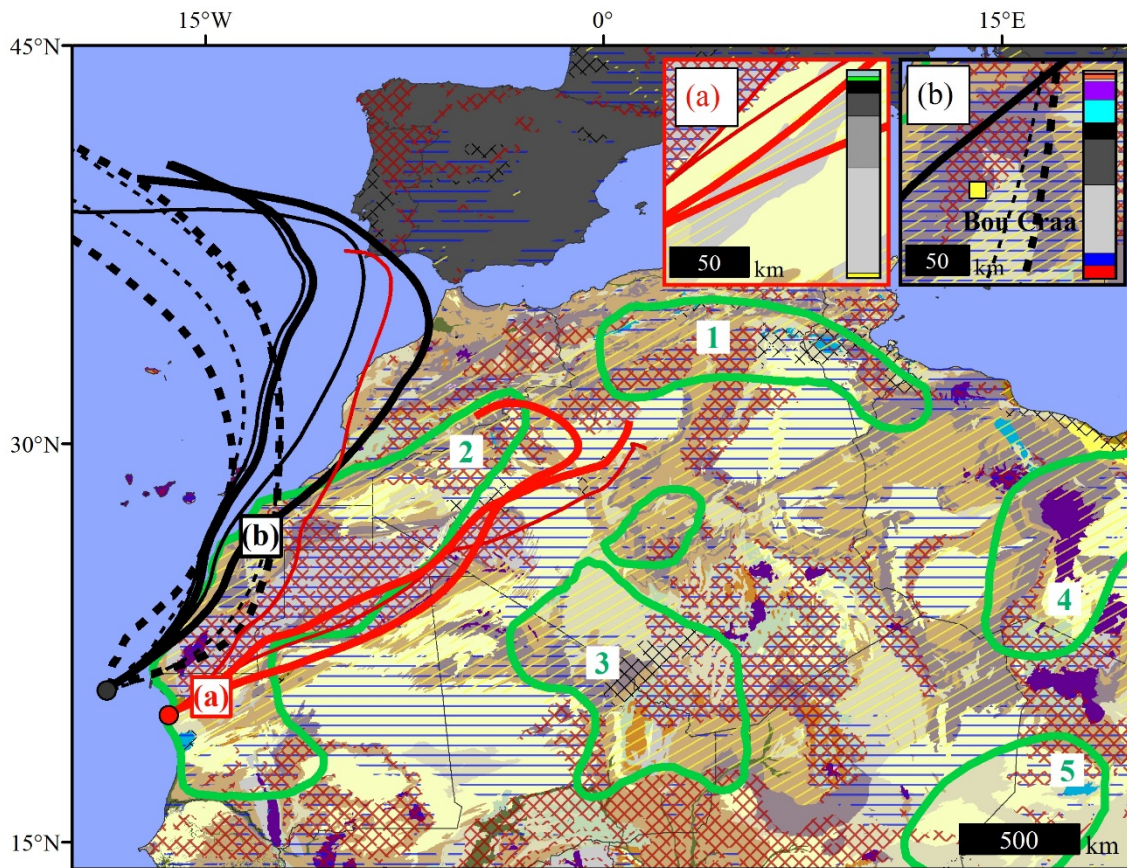
546
 547 **Figure 8: Mineralogical composition (a) averaged over all samples and for sites Iwik and CBI, (b) averaged for the**
 548 **winter samples at sites Iwik and CBI and for each individual winter sample and (c) averaged for the summer samples**
 549 **at sites Iwik and CBI and for each individual summer sample. The category 'other minerals' comprises the minerals**
 550 **todorokite, sodalite, konicklite, guyanaite, nitratnine, urea, bernalite, akermanite, mixed-layer clay and talc.**

551
 552

553 3.5 Identification of dust source regions

554 In Fig. 9-12 the results of the four day back-trajectory analysis are presented for each sample which has been
555 analyzed for mineralogical composition. Four heights, 10 m, 100 m, 3000 m and 4500 m were chosen to cover
556 both low- (trades) and high-level (SAL) dust transport. A back trajectory was drawn for the day when a dust storm
557 event occurred as depicted on satellite images. Only the low-level back-trajectories were plotted for site Iwik
558 because of the correlation of the measured dust characteristics to the low-level wind speed. Moreover, the MWAC
559 samplers were designed to only sample dry deposition, whereas the marine sampling sites collect material settling
560 through the water column, i.e., dust resulting from both dry- and wet deposition. The back-trajectories at 5500 m
561 can be found in the supplement.

562 Figure 9 illustrates a typical late-winter situation. During the sampling interval of each site at least two days with
563 dust storms occurred (Fig. 9c,d). Therefore, two back trajectories were drawn for each height for the site CBi and
564 Iwik respectively. The high-level back trajectories ending at site CBi pass either through the major **PSA 2** or point
565 offshore. Both the low-level back-trajectories ending at the continental trap site Iwik and at the oceanic trap site
566 CBi point to a dust source within the major **PSA 2** (Scheuvens et al., 2013). Some calcite was present in the
567 continental dust sample, but no chlorite nor kaolinite was detected. Therefore, the dust source was most likely
568 located in the nearby southwestern Reguibat Shield where sediments are rich in calcite and quartz and depleted in
569 chlorite and kaolinite (Fig. 9a). Dust deposited in the marine traps during the time interval was characterized by
570 the occurrence of chlorite and kaolinite. Thus, the source area of the samples was most likely the chlorite and
571 kaolinite rich sediments located near the Bou Craa phosphate mine in the Western Sahara (Fig. 9b).

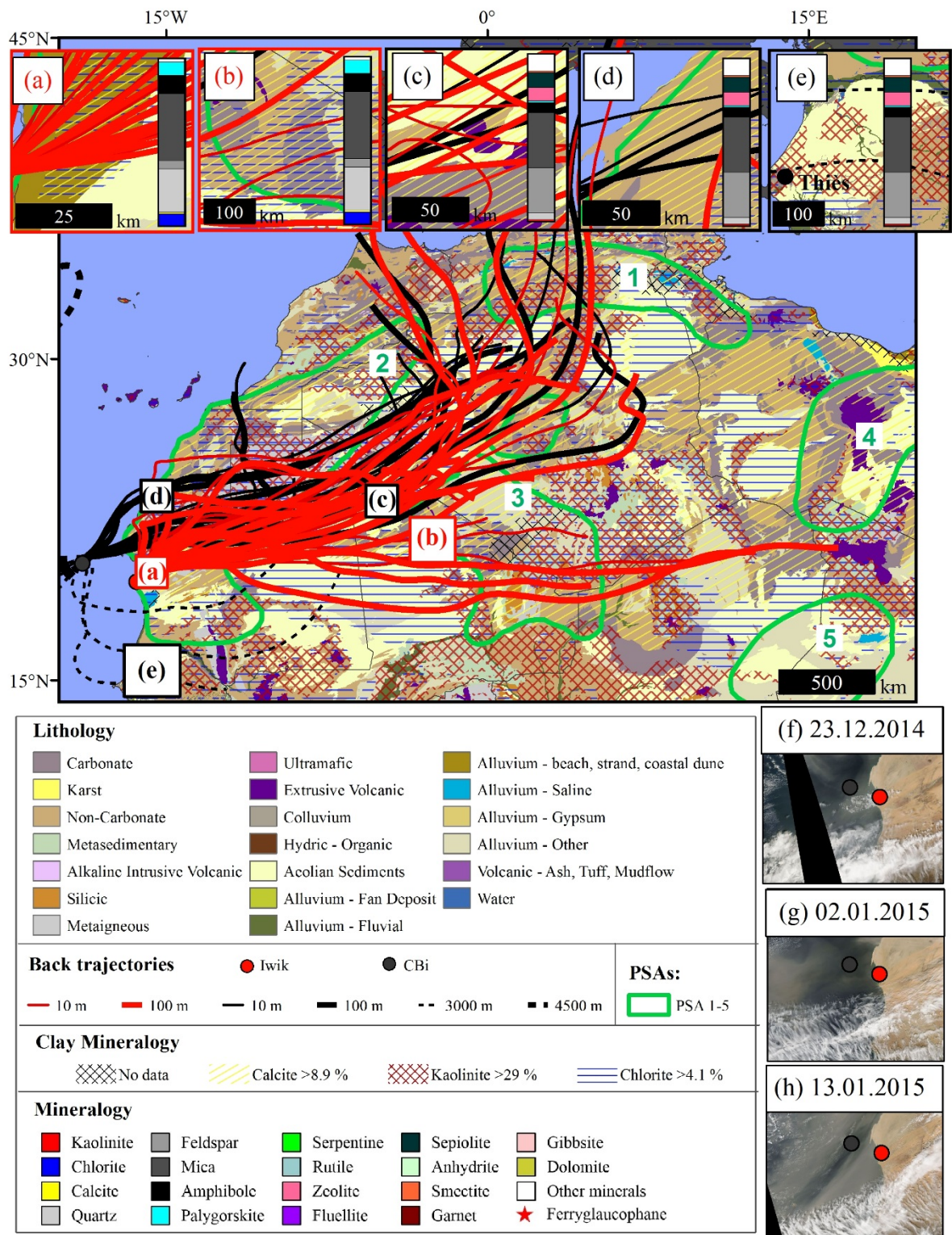


572

573 **Figure 9: Low-level (10 m) four-day back trajectories of dust events ending during the sampling interval 15.02.-15.03.14**
 574 **at site Iwik and during the sampling interval 26.02.-18.03.14 at site CBI. The potential dust source areas and the**
 575 **mineralogy of the samples are given in the subfigures a-b. The dust-storm events occurring during the sampling interval**
 576 **are indicated in subfigures c-d.**

577 Figure 10 represents a typical early-winter situation. During the sampling interval of the site Iwik at least three
 578 dust storms occurred and at the site CBI at least two dust storms occurred (Fig. 10f-h). Each dust storm lasted for

579 several days for which we could model as many as 15 back trajectories for the site Iwik and 8 for the site CBi for
580 each height. The large number of back trajectories complicated the determination of the likely dust source areas.
581 All back trajectories pass through the major **PSA 2** and some point to the **PSA 1** and **3** (Scheuvens et al., 2013).
582 One high-level back trajectory ending at site CBi passes through **PSA 2** and two through Mauritania and Senegal.
583 However, most of the high-level back trajectories ending at site CBi point offshore. Dust sampled in the marine
584 traps during this sampling interval did not contain any chlorite, while the dust trapped at Iwik did. Chlorite may
585 have been supplied to Iwik from a source area nearby the Senegal-Mauritania Basin (Fig. 10a) or as far as the
586 eastern Taoudeni Basin (Fig. 10b) as there are to the anomalously high chlorite content of the soils in these areas.
587 The continental sample is further characterized by the occurrence of calcite and the absence of kaolinite which fits
588 to the soils of the chosen source areas (Fig. 10a,b). The marine sample was characterized by the occurrence of
589 zeolite and absence of chlorite. Therefore, zeolite may have been derived from the extrusive volcanic rocks of the
590 northern Taoudeni Basin (Fig. 10c). A further source area might be the southern shoreline of Western Sahara in
591 which chlorite depleted sediments are situated (Fig. 10d). The presence of the mineral kaolinite in this marine
592 winter sample may be explained by a kaolinite-rich source area lying in the southern Senegal-Mauritania Basin
593 (Fig. 10e).

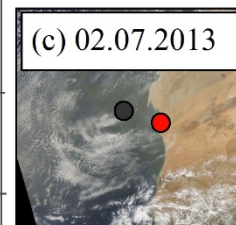
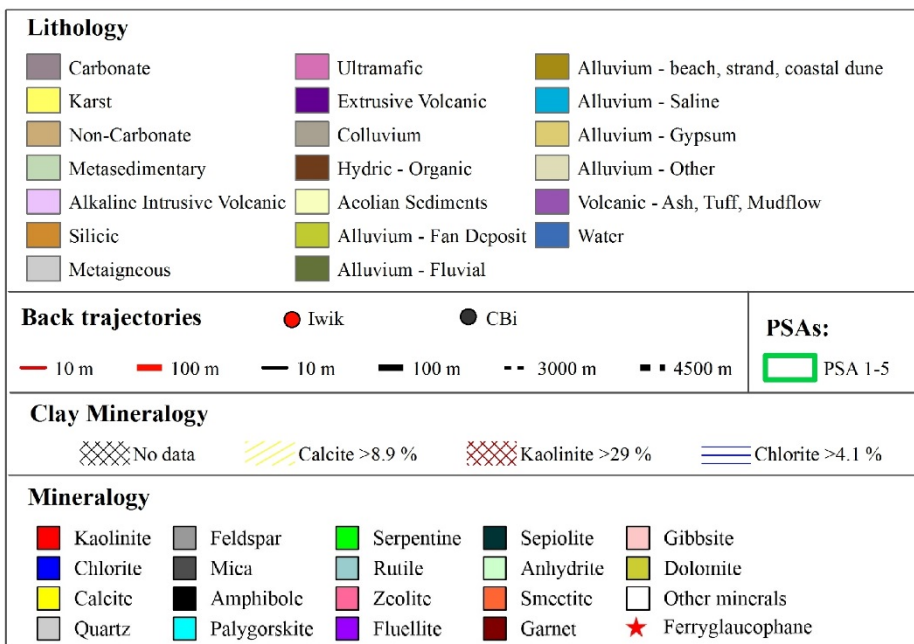
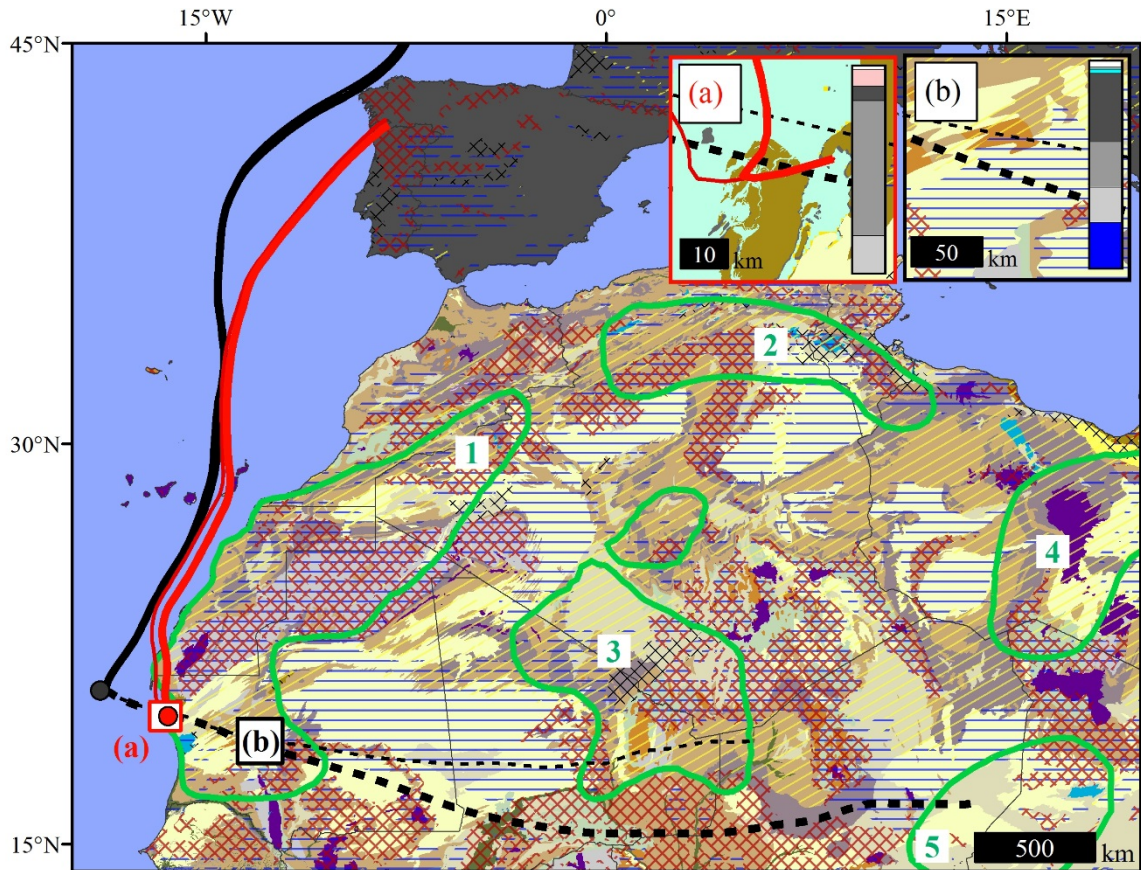


594

595 **Figure 10: Low-level (10 m) four-day back trajectories of dust events ending during the sampling interval 15.12.14-**
 596 **18.01.15 at site Iwik and during the sampling interval 16.12.14-04.01.15 at site CBI. The potential source areas and the**
 597 **mineralogy of the samples are given in the subfigures a-c. The dust storm events occurring during the sampling interval**
 598 **are indicated in subfigures e-g.**

599 In Fig. 11 a typical early-summer situation is presented. Only one dust storm event was observed during the
 600 sampling interval at both sites which lasted for one day (Fig. 11c) resulting in only one back trajectory per site and

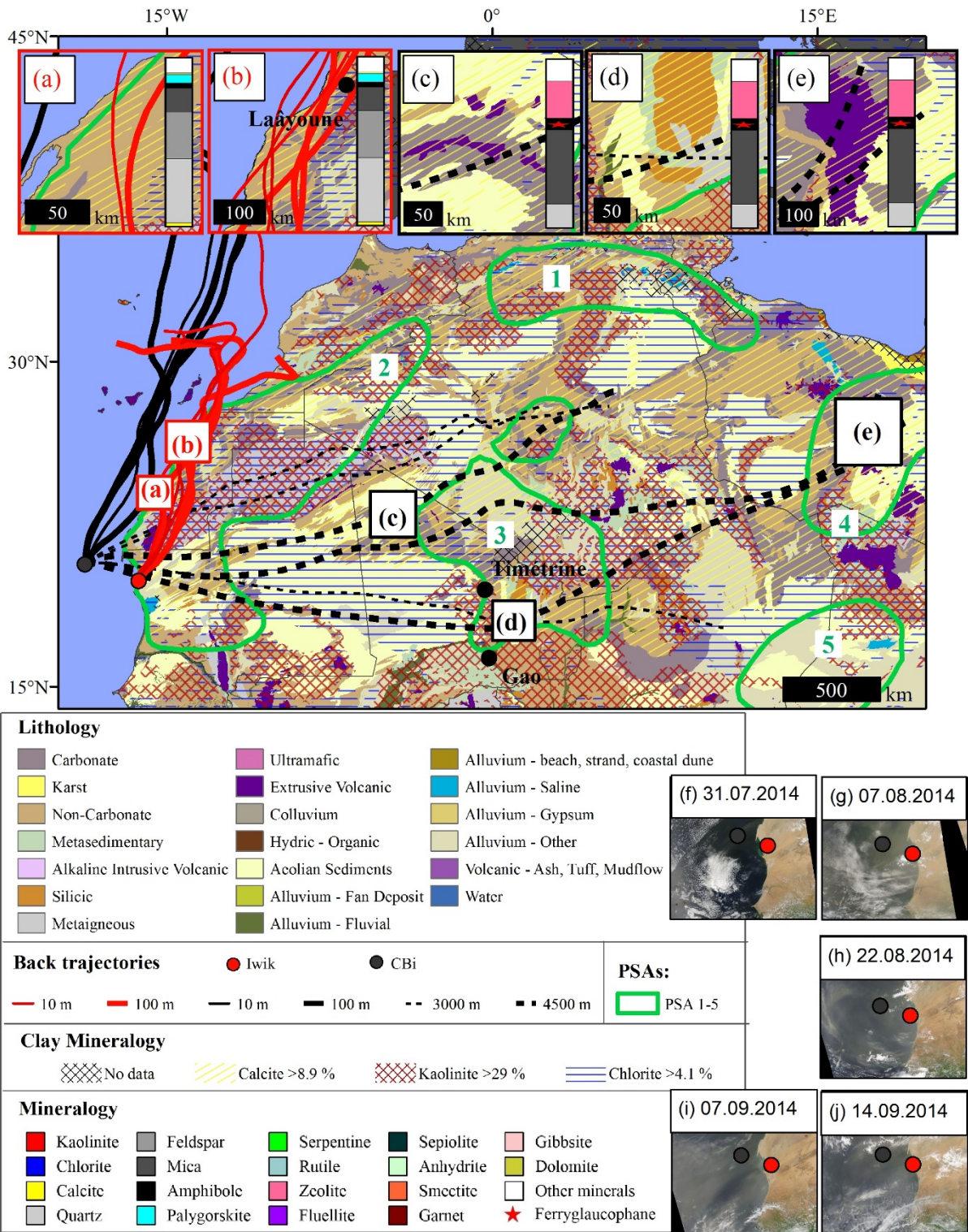
601 per height. The low-level back trajectory ending at site CBI runs offshore and the high-level back trajectory passes
 602 through the major PSA 2, 3 and 5. The low-level back trajectory ending at site Iwik passes through the major PSA
 603 2. (Scheuvens et al., 2013). Dust sampled on land at site Iwik was characterized by the absence of chlorite,
 604 kaolinite and calcite which fits to the soils of northern Tidra Island (Fig. 11a) making it a really local phenomenon.
 605 In contrast, dust sampled offshore at site CBI was characterized by chlorite and by the absence of kaolinite which
 606 fits to the chlorite rich soils in the Mauritanides of Mauritania (Fig. 11b).



607

608 **Figure 11: High- (4500 m) and low-level (10 m) four-day back trajectories of a dust event ending during the sampling**
609 **interval 24.06.-15.07.13 at site Iwik and during the sampling interval 25.06.-16.07.13 at site CBI. The potential source**
610 **areas and the mineralogy of the samples are given in the subfigures a-b. The dust storm event is indicated in subfigure**
611 **c.**

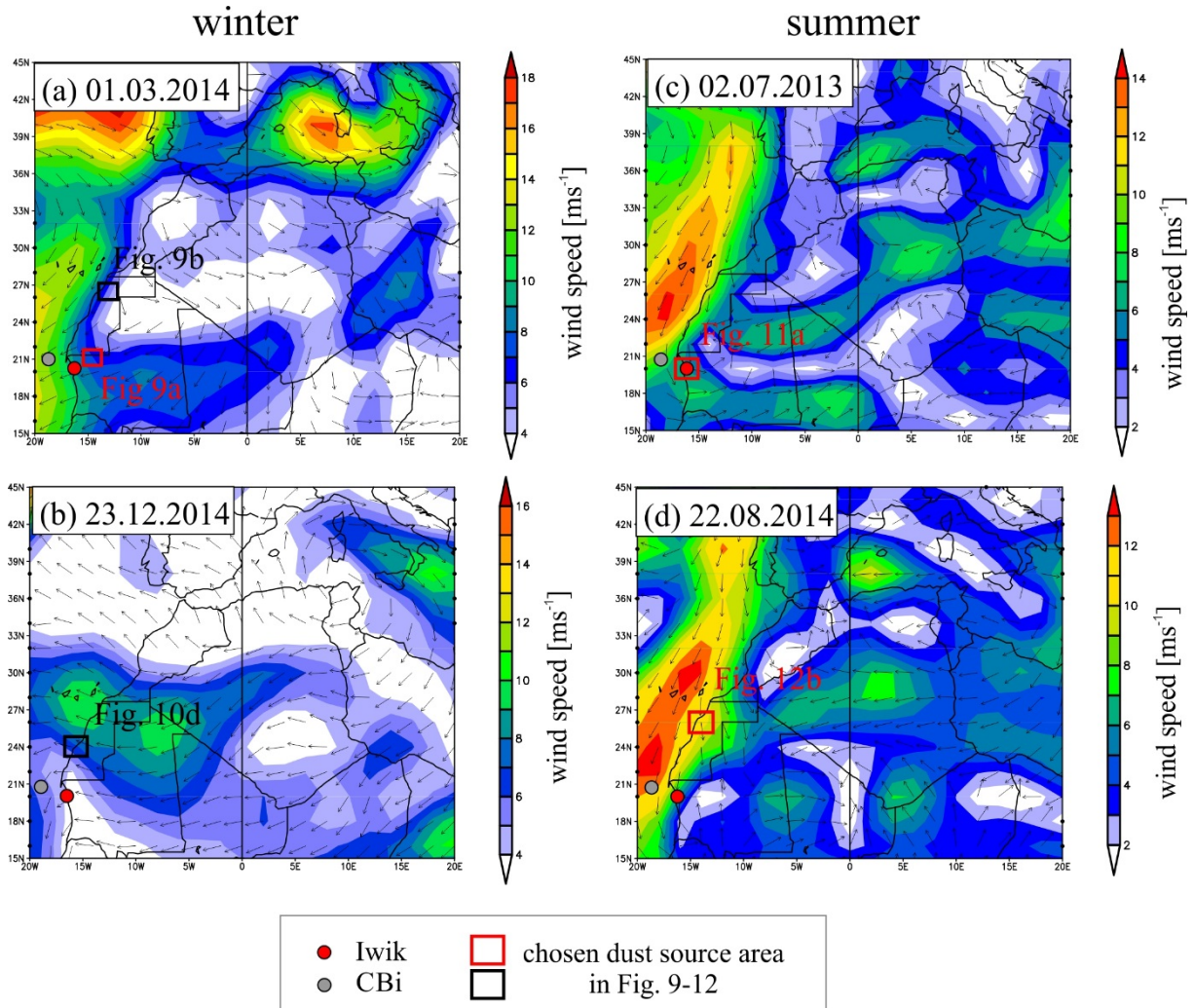
612 In Fig. 12 a typical late-summer situation is illustrated. At least five separate dust events could be identified (Fig.
613 12f-j) out of which three occurred during the sampling interval of the site Iwik and two during the sampling interval
614 of the site CBI. One of these dust storms occurring during the sampling interval of the site CBI lasted for two days
615 (07-08.08.2014), while all other dust storms lasted for only one day. As a result, three back trajectories could be
616 drawn for each site and each height. The low-level back trajectories ending at site CBI run offshore. The low-level
617 back trajectories ending at site Iwik pass through the major **PSA 2**. The high-level back trajectories pass through
618 the major **PSA 2, 3 and 4** (Scheuven et al., 2013). Dust deposited in the continental traps was characterized by
619 the presence of calcite and the absence of chlorite and kaolinite. Therefore, the source area of the dust was most
620 likely in the Western Sahara where soils rich in calcite but poor in chlorite and kaolinite are located (Fig. 12a,b).
621 Dust sampled with the oceanic traps during this sampling interval was characterized by the absence of chlorite and
622 kaolinite and by the presence of a high percentage of zeolite (22 %) (Fig. 8c). Therefore, a possible source area
623 may have been extrusive volcanic rocks of the northern Taoudeni Basin (Fig. 12c) and the Fezzan uplift (Fig. 12e).
624 Ferryglaucofane may have been sourced by the Pharusian belt (Fig. 12d).



625
 626 **Figure 12: High- (4500 m) and low-level (10 m) four-day back trajectories of dust events ending during the sampling**
 627 **interval 15.08.-15.09.14 at site Iwik and during the sampling interval 01.08.-21.08.14 at site CBI. The potential source**
 628 **areas and the mineralogy of the samples are given in the subfigures a-c. The dust storm events are indicated in**
 629 **subfigures e-i.**

630 In Fig. 13a-d the mean wind vectors and speed are presented for chosen dust storm events. The individual dust
 631 source areas that were identified using the back trajectory of the day with the dust storm as shown in Fig. 9-12 are

632 further displayed in Fig. 13a-d. As can be clearly seen in the subfigures, the mean wind velocities were
 633 anomalously large in the chosen dust source areas which enabled dust emission. During winter, six hourly mean
 634 wind velocities were larger than 7 ms^{-1} in the chosen dust source areas (Fig. 13a-b). During summer 2013, six
 635 hourly mean wind velocities were larger than 6 ms^{-1} in the chosen dust source area (Fig. 13c). During summer
 636 2014 extremely high mean wind velocities were encountered near the study sites and in the dust source area
 637 enabling dust emission and transport from a more distant source to the site Iwik (Fig 13d).



638
 639 **Figure 13: Six hourly composite mean wind vectors and speed at 1000 mb for selected days including a dust**
 640 **storm event during winter (a) – (b) and summer (c) – (d). The dust source area that was identified for the**
 641 **individual dust storm event using the back trajectory of the day with the dust storm is further displayed.**

642
 643
 644
 645
 646
 647

648 4. Discussion

649 4.1 Comparison of dust collected on land and in the ocean

650 4.1.1 Dust concentrations

651 An annual average dust concentration (total suspended particles) of ~ 214 and $275 \mu\text{gm}^{-3}$ was estimated for all dust
652 samples of the year 2013 and 2014 respectively regarding the site Iwik (Table 5). These estimates were larger than
653 what has been measured for background dust concentrations (total suspended particles) in Morocco which were in
654 the order of $100 \mu\text{gm}^{-3}$ during spring 2006 (Kandler et al., 2009). However, in Morocco dust was collected at a
655 larger height of 4 m and haze-periods and dust-storms were excluded from the average value. The horizontal dust
656 fluxes at site Iwik correlated positively to wind speed (Fig. 7b) and decreased with collection height (not shown).
657 This underscores the proximity of this continental site to the dust emission source.

658 At the distal oceanic site CB, the annual average dust deposition flux was $\sim 45 \text{mgm}^{-2}\text{d}^{-1}$ (2013) (Table 5). The
659 dust flux was slightly larger than the average annual dust flux observed at site CB between 1988 and 2012 with \sim
660 $30 \text{mgm}^{-2}\text{d}^{-1}$ (Fischer et al., 2015b). The slightly larger dust fluxes may have been caused by the anomalously high
661 frequency in dust storm events as observed on satellite images occurring during the studied time period (not
662 shown). The observed general decrease in the dust flux from the site Iwik to the sites CBi and CB can be explained
663 via the increase in the distance to the source area. Decreased dust deposition fluxes offshore NW Africa with
664 increasing distance from the African coast were also observed by Bory and Newton (2000) analysing the lithogenic
665 fluxes in marine sediment traps.

666 The average horizontal fluxes at site Iwik were ~ 1000 times larger with $\sim 100000 \text{mgm}^{-2}\text{d}^{-1}$ (Table 5) due to the
667 different sampling technique. The MWAC samplers do not measure deposition fluxes but foremost dust
668 concentrations. Only 1% or less drops out of a moving dust cloud within five minutes, hence, the horizontal dust
669 flux is at least ~ 100 times higher than the dust deposition flux (Goossens, 2008). The fact that the dust fluxes
670 decreased with height (not shown) further complicated a comparison between the sites due to the different
671 sampling heights of the dust collectors (2.90 m at Iwik versus sediment traps in the water). Therefore, the fluxes
672 between the site Iwik and the offshore sediment trap moorings cannot be compared.

673 4.1.2 Dust transport

674 The measured grain-size distributions for dust trapped at 2.90 m on land at site Iwik and for dust settling in the
675 ocean were predominantly unimodal (Fig. 6). Unimodal grain-size distributions are typical for wind-blown
676 sediments (Pye, 1995). Unimodal grain-size distributions were also measured for dust deposited in a vertical dust
677 sampler in M'Bour (Skonieczny et al., 2011), dust sampled on ship vessels (Stuut et al., 2005) and in other
678 sediment trap samples offshore NW Africa (Ratmeyer et al., 1999b; Van der Does et al., 2016; Friese et al., 2016).

679 The measured annual average modal grain size at site Iwik was $48 \mu\text{m}$ (Table 5). The obtained average annual
680 modal grain size was close to the large coarse mode population of $44 \mu\text{m}$ observed by Gillies et al. (1996) for dust
681 trapped at a height of 10 m during spring in Fakarbé (Mali) which is located about 700 km southeast of Iwik.
682 Gillies et al. (1996) conclude that the large coarse mode population in the dust samples points to locally-derived
683 dust. Based on this observation, we argue that also the dust trapped near Iwik was most likely generally of regional
684 instead of long-distance provenance. The distance to the main source area may be, however, not in the direct

685 surrounding of the dust collector since dust sampled with MWAC samplers in the vicinity of barchan dunes of the
686 Bodélé depression at 2.4 m height is characterized by a larger modal particle size of $\sim 100 \mu\text{m}$ (Chappell et al.,
687 2008). The annual average modal and maximum particle size gradually decreased from the on-land site Iwik, to
688 the proximal oceanic site CBI and the distal oceanic site CB (Table 5, Fig. 6a). This decrease in particle size
689 between the stations CB and CBI was observed before and was attributed to the preferred gravitational settling of
690 coarse particles during dust transport (Friese et al., 2016). Moreover, many studies have confirmed a downwind
691 fining of the terrigenous fraction of surface sediments offshore NW Africa (Koopmann, 1981; Holz et al.,
692 2004; Fütterer, 1980; Raczewski, 1939; Lange, 1975), and it is intuitively logical.

693 Bimodal grain-size distributions typically indicate the sampling of different dust sources (Stuut et al. (2009) and
694 references therein). The three samples of the Iwik time series that were characterized by an additional small peak
695 in the grain-size distribution around $\sim 16 \mu\text{m}$ were sampled during sampling intervals of anomalously high wind
696 velocity. The back-trajectories of one of these samples pointed towards a proximal and more distal dust source
697 (Fig. 12a,b). Therefore, it may be possible that wind velocities were high enough during the sampling interval to
698 inject dust to higher altitude and transport it from more distant sources (Fig. 12b) to the sampling site resulting in
699 the small peak in the grain-size distributions. This interpretation is further supported by the reanalysis wind vector
700 maps showing anomalously high wind velocities between the site Iwik and the proposed distant source area enabling
701 dust emission and transport of dust particles from more distant source to the site Iwik (Fig. 13d). On the other
702 hand, microscopic examination prior to particle-size analyses of the Iwik samples revealed that the samples
703 included many aggregates (Fig. 5d). Hence, locally derived aggregates may have been sampled during periods of
704 high wind velocities. These aggregates may have been dispersed in the demineralized water during the
705 measurement of the laser resulting in the observed additional smaller coarse mode population at $\sim 16 \mu\text{m}$. Further,
706 precipitation was encountered according to the TRMM data during the sampling interval of two of these three
707 samples. Therefore, a further explanation for the bimodal grain-size distributions may be the deposition of dust
708 particles with a mode of $\sim 16 \mu\text{m}$ from higher altitude of the SAL due to precipitation. The rain droplets may have
709 evaporated during their fall releasing the dust particles at lower altitudes which can then be sampled with the
710 MWAC sampler. However, we also observed remnants of water in the bottles and therefore wet deposition into
711 the bottles may have also occurred. During summer, frequent rainfall resulted in a decrease of the modal particle
712 size of deposited Saharan dust at site Iwik (Fig. 7c). In addition, the seasonal average percentage of PM₁₀ particles
713 was larger during summer compared to winter at the site Iwik and CBI (Tab.5). These observations may also be
714 explained by the deposition of relatively finer dust particles from higher altitude of the SAL during summer due
715 to precipitation. One winter and one summer sample of the oceanic samples that were characterized by bimodal
716 grain-size distributions have several proposed dust source areas each (Fig. 10, 12). Thus, the sampling of long- as
717 well as short-travelled dust may have resulted in a bimodal grain-size distribution.

718 Both at the onshore sampling site Iwik and at the offshore sampling site CBI a clear seasonal trend in the particle
719 sizes of deposited dust could be observed with generally coarser modal particle sizes during summer compared to
720 winter (Fig. 6b,c). Generally coarser summer modal particle sizes of deposited dust at site CBI were observed
721 before for a three year time series during 2003 to 2006 and related to moist convective events (Friese et al., 2016).
722 The generally coarser particle sizes during summer at the site Iwik compared to winter may be explained by the
723 trade-wind speed as a positive correlation between the modal grain sizes and surface wind velocities was observed
724 (Fig. 7a), This implied that dust was transported with the trade winds from sources of a quite constant distance

725 year-round. During dust-storm events particles with a diameter of 40 to 50 μm may be transported \sim 100 km (Tsoar
726 and Pye, 1987). The proposed source areas all fall in this range except for the winter sample of 2014-2015 (Fig.
727 10). The winter sample was characterized by an anomalously low modal grain size of 38 μm and particles of this
728 size may be transported more than 100 km during dust storm events (Tsoar and Pye, 1987). Moreover, Van der
729 Does et al. (2016) observed how particles up to 100 μm were transported \sim 3500 km across the Atlantic Ocean.
730 To sum up, the seasonal variability in the modal particle size of deposited dust at the site Iwik was mainly driven
731 by the surface wind speed due to the predominant sampling of nearby dust sources year-round.

732 **4.1.3 Dust mineralogical composition**

733 In the dust sampled at Iwik the minerals quartz, feldspar, mica, amphibole, palygorskite, chlorite, calcite, dolomite,
734 gibbsite, rutile and serpentine were present (Fig. 8a). The observed occurrence of the minerals quartz, feldspar,
735 mica, chlorite and calcite has also been described for the bulk size fraction of soil samples and dust samples
736 collected in Mauritania (Schütz and Sebert, 1987). Palygorskite, mica and chlorite have also been detected by
737 Skonieczny et al. (2013) in the PM_{30} size fraction of a three-year time series of dust deposition at M'Bour, Senegal,
738 more than 500km south of Iwik, Mauritania. Smectite and kaolinite, which were absent in the Iwik samples, were
739 the dominant minerals of the dust sampled at M'Bour (Skonieczny et al., 2013). Smectite and kaolinite are
740 considered as indicative for wet tropical soils and their relative abundance in soils increases southwards along the
741 northwest African coast (Lange, 1982; Biscaye, 1964). We argue that the mineralogical differences between the
742 two sites are explained by the >500 km distance between Iwik and M'Bour and the fact that the latter station is
743 surrounded by tropical soils. Gibbsite, rutile and serpentine have not been reported in any continental dust study
744 so far and thus seem to be indicative for locally-derived dust (Fig. 9a, Fig. 11a).

745 The dust sampled at the proximal marine site CBI contained the minerals quartz, feldspar, mica, amphibole,
746 palygorskite, chlorite, zeolite, kaolinite, smectite, sepiolite, rutile, garnet, anhydrite and fluellite (Fig. 8a). The first
747 seven of these minerals were also found in the clay and/or silt and sand fraction of Saharan dust sampled during
748 ship cruises parallel to the coast about 70 km off Cape Blanc (Chester et al., 1971) and perpendicular to the coast
749 about 80 to 180 km off Cape Blanc (Chester and Johnson, 1971b). Analogous to the samples of this study, the
750 PM_{20} fraction of surface sediments of the piston cores RC05-57, RC05-60 and A180-44 also feature zeolites and
751 the surface sediments of core RCRC05-57 also traces of pyrophyllite (sepiolite belongs to the pyrophyllite group)
752 (Biscaye, 1964). Further, rutile was also present in the silt and sand fraction of Saharan dust sampled perpendicular
753 to the coast on the research vessel (Chester and Johnson, 1971b). Palygorskite was found in the clay fraction of
754 the surface sediment of sediment core GIK12329 ($19^{\circ} 22' \text{ N}$, $19^{\circ} 56' \text{ W}$) offshore Cape Blanc and is considered a
755 characteristic mineral of Saharan dust (Lange, 1975). The observed annual average C/K ratio ($C/K=4$) recorded
756 for the bulk size fraction of the trap samples was larger than the C/K ratio ($C/K=0.3-1$) recorded in the clay fraction
757 of surface sediment samples offshore Cape Blanc by Lange (1982). The disagreement may be due to the generally
758 larger percentage of kaolinite in the clay fraction compared to the silt fraction (Journet et al., 2014).

759
760 The dust samples of the site Iwik were further characterized by a dominance in quartz and feldspar (Fig. 8a). A
761 dominance in quartz has also been described for continental dust samples and soil samples collected in Mauritania
762 by Schütz and Sebert (1987). More than 20 papers published XRD data of northern African dust reporting quartz
763 as the main mineral in most dust samples (Scheuven et al., 2013). The observed increase in micas and decrease
764 in quartz and feldspar observed for the marine samples relative to the Iwik samples (Fig. 8a) can be explained via

765 the preferential gravitational settling of the larger dust minerals quartz and feldspar during transport (Delany et al.,
 766 1967;Glaccum and Prospero, 1980;Chester and Johnson, 1971b;Schütz and Sebert, 1987). A strong downwind
 767 decrease in quartz content in Saharan dust was also observed by Korte et al. (2017).

768

769 **4.2 Mineralogy as a provenancing tool**

770

771 In Table 7 an overview of the chosen dust source areas for the site Iwik and CBi is given together with the
 772 characteristic minerals of the samples that may be used as a tracer for the source area. In the following subsections
 773 the identification of the source areas and mineralogical tracers is described in detail.

774 **Table 7: Overview of the chosen source areas and the tracer minerals of the individual samples together with the given**
 775 **characteristics of the source areas according to literature. ‘**

Sampling interval	Characteristic minerals of sample	Chosen dust source area	Bulk mineralogical composition of chosen PSA ⁽¹⁶⁾	Characteristic source rocks and deposits of chosen source area
Iwik				
15.02.- 15.03.14	*Rut, Serp, Cc	PSA 2: Reguibat Shield	C/K = 0.0–1.0 *Pal: 1-30 wt%	Metamorphic and granitic rocks ⁽¹⁾ Serpentinities ⁽²⁾
15.12.14- 18.01.15	*Cc, Chl, Pal (8 wt. %)	PSA 2: Senegal-Mauritania Basin	C/K = 0.0–1.0 *Pal: 1-30 wt%	Chalky horizons ⁽³⁾
		PSA 3: Eastern Taoudeni Basin	C/K = 0.2–0.9 *Pal: 1-5 wt%	Carbonate sequences ⁽⁴⁾
24.06.- 15.07.13	*Gib	PSA 2: Tidra Island	C/K = 0.0–1.0 *Pal: 1-30 wt%	Gibbsite maximum offshore Cape Blanc ⁽⁵⁾
15.08.- 15.09.14	*Cc, Dol, Pal (5 wt. %)	PSA 2: Aaiun-Tarfaya Basin	C/K = 0.0–1.0 *Pal: 1-30 wt%	Limestone deposits ⁽⁶⁾ Outcrops near Laâyoune with dolomites ⁽⁶⁾
CBi				
26.02.- 18.03.14	*Chl, Kao (C/K = 1), Pal (11 wt. %), Flu, Anh, Sme, Ga	PSA 2: Aaiun-Tarfaya Basin near Boucraa	C/K = 0.0–1.0 *Pal: 1-30 wt%	Phosphate deposits ⁽⁷⁾
16.12.14- 04.01.15	*Kao (C/K = 0), Pal (1 wt. %), Zeo, Se, Sme	dike swarms and sills of northern Taoudeni Basin	-	Basalts with glass ⁽⁹⁾
		PSA 2: Aaiun-Tarfaya Basin	C/K = 0.0–1.0 *Pal: 1-30 wt%	Palygorskite-sepiolite mafic clays ⁽¹⁰⁾
		Southern Senegal-Mauritania Basin	-	Lateritic soil ⁽⁸⁾ Horizontal layers of palygorskite and sepiolite ⁽⁸⁾
25.06.- 16.07.13	*Chl, Pal (2 wt. %), Rut	PSA 2: Mauritanides	C/K = 0.0–1.0 *Pal: 1-30 wt%	Strongly metamorphosed rocks ⁽¹⁰⁾ Greenschist facies ⁽¹¹⁾
01.08.- 21.08.14	*Fe-Amf, Zeo	dike swarms and sills of northern Taoudeni Basin	-	Basalts with glass ⁽⁹⁾
		PSA 4: Fezzan uplift	C/K = 0.0–2.6 *Pal: 0 wt%	Zeolite in basaltic rocks ^(12,13)
		PSA 3: Pharusian belt	C/K = 0.2–0.9 *Pal: 1-5 wt%	Blueschists ⁽¹⁴⁾ Glaucofane bearing eclogites ⁽¹⁵⁾
* Amf = amphibole, Pal = palygorskite, Chl = chlorite, Cc = calcite, Dol = dolomite, Gib = gibbsite, Zeo = zeolite, Kao = kaolinite, Sme = smectite, Se = sepiolite, Rut = rutile, Serp = serpentine, Ga = garnet, Anh = anhydrite, Flu = fluellite				
⁽¹⁾ Schofield et al. (2006) and references therein ⁽²⁾ Schlüter (2008) ⁽³⁾ Wissmann (1982) ⁽⁴⁾ Bertrand-Sarfati et al. (1991) ⁽⁵⁾ Biscaye (1964) ⁽⁶⁾ Bosse and Gwosdz (1996) ⁽⁷⁾ Moreno et al. (2006) ⁽⁸⁾ García-Romero et al. (2007) ⁽⁹⁾ Verati et al. (2005) ⁽¹⁰⁾ Villeneuve (2005), ⁽¹¹⁾ Dallmeyer and Lécorché (2012) ⁽¹²⁾ Abdel-Karim et al. (2013) ⁽¹³⁾ Cvetković et al. (2010) ⁽¹⁴⁾ Caby (2014), ⁽¹⁵⁾ Caby et al., (2008) ⁽¹⁶⁾ Scheuven et al. (2013)				

776

777 **4.2.1 Dust collected on land**

778 The variability of the mineralogical composition of dust sampled at the site Iwik could be related to the synoptic
779 scale change in the surface trade wind direction. However, meteorological data from nearby sites like e.g.
780 Nouadhibou demonstrate that local effects like the topography exert a strong influence on observed wind directions
781 at ground level (Fig. 2). The back trajectories indicate that the dust sources for the dust collected in Iwik during
782 winter were located NE and E of the sampling site (Fig. 9a, Fig.10a,b), while those during summer were located
783 W (within the PNBA) and NNE of the sampling site (Fig. 11a, Fig. 12a,b). This is in accordance with a change in
784 the dominant local surface wind direction from NE in winter to NNE in summer (Fig. 2) and is also reflected in
785 the clay-mineralogical composition of the samples.

786 Generally, there is not much variability in the clay-mineralogical composition of the Iwik samples. The back
787 trajectories for the winter sample of 2014 indicate that the material was blown from the southwestern Reguibat
788 Shield (**PSA 2**) (Fig. 9a). The lack of palygorskite in this sample does not fit to the proposed bulk palygorskite
789 content (1-30 %) of **PSA 2** (Scheuven et al., 2013) (Table 7). Therefore, we argue that the sampled dust was most
790 likely derived from a localized source of **PSA 2**. The sample included the characteristic minerals rutile and
791 serpentine (Table 7) which are usually a result of metamorphic processes (Deer et al., 1992). Indeed, the western
792 Reguibat Shield is composed of metamorphic and granitic rocks (Schofield et al. (2006) and references therein)
793 and the rocks are intruded by serpentinites (Schlüter, 2008). The sample was further characterized by the highest
794 quartz percentage among all samples (~ 50 %) (Fig. 8b). The sand dunes of the Azefal sand sea which cover part
795 of the southwestern Reguibat Shield might have sourced these quartz grains (Fig. 9a). The sand dunes may have
796 been fed by outcropping carbonate deposits at the northern rim of the Taoudeni Basin via the NE-trade winds
797 leading to anomalously high percentages of calcite in the sand dunes (Fig. 9). Thus, the sand dunes may have also
798 sourced the calcite present in the sample (Fig. 8b).

799

800 The winter sample of 2014-2015 was suggested to be sourced from sediments of the northern Senegal-Mauritania
801 Basin (**PSA 2**) (Fig. 10a) and the eastern rim of the Taoudeni Basin (**PSA 3**) (Fig 10b). The palygorskite content
802 of the sample (8 %) fits to the proposed bulk palygorskite content of **PSA 2** (Scheuven et al., 2013) (Table 7).
803 This may point to several externally mixed sources of **PSA 2** during transport.

804 The sample was further characterized by calcite and chlorite (Table 7). The sediments in the northern Senegal-
805 Mauritania Basin (Fig. 10a) comprise Quaternary chalky horizons (Wissmann, 1982) which may have sourced the
806 calcite. More likely, calcite may have been derived from the Mesozoic carbonate sequences cropping out in the
807 eastern rim of the Taoudeni Basin (Bertrand-Sarfati et al., 1991) (Fig. 10b). A source area lying at the
808 Algerian/Mali border was also suggested for a chlorite and calcite bearing dust sample collected on the Canary
809 Islands (Alastuey et al., 2005). The winter dust sample trapped at site Iwik was further characterized by the lowest
810 feldspar percentage (~ 5 %), highest mica percentage (~ 40 %) (Fig. 8b) and lowest modal grain size (~ 38 μm)
811 among all Iwik dust samples analysed for mineralogy. The Stokes terminal settling velocity is smaller for platy
812 particles than for spherical particles of similar diameter (Santamarina and Cho, 2004). Therefore, a long-distance
813 transport of dust from the eastern Taoudeni Basin to Iwik may have resulted in a depletion in spherical quartz
814 particles (Fig. 5a,b,c) and an enrichment in platy mica particles (Fig. 5b).

815

816 The summer sample of 2013 was proposed to be sourced from the near-by northern Tidra Island (**PSA 2**) (Fig.
817 11a). Again, the absence of the mineral palygorskite is noteworthy which may point to the sampling of a localized
818 dust source.

819 The sample was further characterized by the mineral gibbsite (Table 7). The northern Tidra Island is famous for
820 the local occurrence of west Africa's northernmost mangroves (Proske et al., 2008) which grow in humid and
821 warm climates. Humid and warm conditions are also beneficial for the formation of gibbsite which forms through
822 tropical weathering (Deer et al., 1992). Therefore, we argue that the soils of Tidra Island supplied the gibbsite
823 found in the sample. A localized small gibbsite maximum was outlined for the surface sediments offshore Cape
824 Blanc (Biscaye, 1964) which further supports the view that gibbsite is supplied from a local source. The sample
825 was further characterized by anomalously large moderately spherical quartz grains (Fig. 5c) emphasizing a short
826 travel distance of the dust.

827

828 The summer sample of 2014 was most likely sourced by sediments of the Western Sahara (**PSA 2**) (Fig. 12a,b).
829 The palygorskite content of the sample (5 %) matches with the proposed bulk palygorskite content of **PSA 2**
830 (Scheuvens et al., 2013) (Table 7). Hence, dust may have been supplied from several dust sources of **PSA 2** which
831 were mixed during transport.

832 The sample was further characterized by calcite and dolomite (Table 7). Sediments outcropping in the Western
833 Sahara are composed of Tertiary sediments (Wissmann, 1982) with limestone deposits (Bosse and Gwosdz, 1996)
834 that may explain the calcite found in the sample (Fig., 12a). Upper cretaceous outcrops in the Aaiun-Tarfaya Basin
835 near Laâyoune comprise dolomites (Bosse and Gwosdz, 1996) and could have sourced the dolomite found in the
836 sample (Fig. 12b). A further evidence for dolomite-bearing dust transport from the Aaiun-Tarfaya Basin is a local
837 dolomite maximum outlined for the surface sediments offshore the Western Sahara (Johnson, 1979). A Saharan
838 dust sample trapped in NE Spain also contained dolomite and calcite and was related to a source area lying in the
839 Western Sahara (Avila et al., 1997).

840

841 **4.2.1 Dust collected at the marine sites**

842 The seasonal contrast in the dust transport patterns (high-level Saharan Air Layer vs. low-level Trades) potentially
843 led to strongly deviating dust sources for the material deposited in the marine trap samples. During winter, the
844 back trajectories indicated that the potential dust source areas were located NE of the sampling site (Fig. 9b, Fig.
845 10c,d), while those during summer were located NE, E and SE of the sampling site (Fig. 11b, Fig. 12a,c,d,e). This
846 large variability in wind patterns can clearly be recognized in the clay-mineralogical compositions of the samples
847 throughout the seasons.

848 Considering the much larger catchment area of the traps, several dust sources may have been sampled with the
849 traps. As a result, the composition of the analyzed samples fit well to the bulk composition of the chosen **PSA**.
850 The back trajectories indicate that the winter sample of 2014 originated from the shoreline of the Western Sahara
851 (**PSA 2**) (Fig. 9b). The observed C/K ratio (C/K=1) and the palygorskite content (11 %) are in agreement with the
852 bulk compositional C/K ratio (C/K=0-1) and palygorskite content of **PSA 2** (Scheuvens et al., 2013) (Table 7).

853 The sample was further characterized by the presence of garnet, fluellite and anhydrite (Table 7). The
854 characteristic occurrence of garnet together with the highest quartz content (33 %, Fig. 8b) among all CBI samples
855 confirms a short transport distance of the trapped dust. The mineral fluellite which is a weathering product of

856 phosphate may have been derived from outcropping phosphate deposits near the Bucraa phosphate mine (Moreno
857 et al., 2006) (Fig. 9b). Anhydrite could originate from evaporites along the coast.

858

859 The back trajectories of the winter sample of 2014 to 2015 lead to the Reguibat Shield (**PSA 2**) (Fig. 10c) and
860 coastal Western Sahara (**PSA 2**) (Fig. 10d). The observed C/K ratio (C/K=0) and palygorskite content (1 %) fall
861 within the ranges of these minerals in **PSA 2** (Scheuvens et al., 2013) (Table 7).

862 The sample was further characterized by the mineral zeolite, kaolinite, sepiolite and smectite (Table 7)). Zeolites
863 are formed from volcanic glass and tuff and form well-developed crystals in basalts (Deer et al., 1992). Therefore,
864 the source area of the zeolites may have been outcropping volcanic rocks in the northern Taoudeni Basin (Fig.
865 10c). These rocks belong to mafic dikes and sills which are commonly basalts with dotted patches of glass (Verati
866 et al., 2005). An additional indication for a distant dust source may be the lowest quartz content (4 %) among all
867 samples (Fig. 8b). Palygorskite-sepiolite mafic clays were found in soil samples of the Western Sahara (Moreno
868 et al., 2006) which may supports a Western Saharan source (Fig. 10d).

869 Sepiolite belongs to the pyrophyllites which is a mineral that also may be considered indicative of tropical
870 weathering (Moore and Reynolds, 1989). Moreover, kaolinite is usually considered indicative of tropical
871 weathering and the laterites of the southern Sahara and Sahel (Lange, 1975;Biscaye, 1964;Lange, 1982). Outcrops
872 of quaternary laterites as well as outcrops of lower Eocene horizontal layers of palygorskite and sepiolite were
873 described near Thiès in Senegal (García-Romero et al., 2007). Therefore, the kaolinite-rich soils and outcrops in
874 the southern Senegal-Mauritania basin near Thiès (Fig. 10e) may have served the kaolinite, sepiolite and
875 palygorskite found in the sample.

876 Another explanation for the presence of kaolinite and smectite in the sample may be the transport of these minerals
877 from southern latitudes via the poleward-flowing undercurrent to the trap site CBi (Fig. 1). Kaolinite and smectite
878 were found in the clay fraction of the surface sediments off Senegal (Nizou et al., 2011) and may have been brought
879 into the ocean by the Senegal River, and redistributed by ocean currents (Biscaye, 1964). The season of high
880 Senegal River sediment supply is between July to October/November (Gac and Kane, 1986). Assuming a mean
881 speed of ~10 cm/s of the undercurrent (Mittelstaedt, 1991), it may take about two months for the particles to travel
882 a distance of ~500 km to the trap site CBi. This time delay might explain the observed occurrence of these minerals
883 in the trap samples during winter, but not during summer.

884

885 Based on the back trajectories, the summer sample of 2013 was suggested to be sourced from the Mauritanides
886 (**PSA 2**) (Fig. 11c). This is confirmed by the palygorskite content of the sample (2 %) (Scheuvens et al., 2013)
887 (Table 7). Outstanding minerals in this sample are chlorite and rutile (Table 7). Outcrops in the Mauritanides west
888 of the Taoudeni Basin feature strongly metamorphosed rocks (Villeneuve, 2005) and greenschist facies (Dallmeyer
889 and Lécorché, 2012) which may have been the source of the rutile and chlorite.

890

891 The reconstructed source area of the summer sample of 2014 was the Pharusian belt (**PSA 3**) (Fig. 12c), the
892 extrusive volcanics of the northern Taoudeni Basin (**PSA 2**) (Fig. 12d) and the Fezzan uplift (**PSA 4**) (Fig. 12e).
893 The lack of palygorskite in the sample does corroborate with **PSA 4** ('not detected') (Scheuvens et al., 2013)
894 suggesting that the provenance of the dust sample may be mainly confined to **PSA 4** (**Table 7**). The sample was
895 further characterized by zeolite and ferryglaucophane (Table 7). The dike swarms and sills of the northern
896 Taoudeni Basin (Verati et al., 2005) (Fig. 10c, Fig. 12c) and/or the basalts of the Fezzan uplift (Fig. 12e) may have

897 sourced the zeolite. Indeed, zeolite was described as one of the main secondary minerals in the basaltic rocks of
898 the central Al-Harui Al-Abyas basalt flows (Abdel-Karim et al., 2013) and in vesicles of the east Al Haruj basalts
899 (Cvetković et al., 2010) of the Fezzan uplift. Traces of zeolite were also detected in the Iwik sample during this
900 sampling interval. It may be that the zeolite dropped out of the high-altitude dust cloud and was subsequently
901 transported via the surface trade winds to the continental trap site. The presence of ferryglaucophane and the
902 absence of feldspar and chlorite in the sample indicates highly metamorphous outcrops constituting the dust source.
903 Therefore, the sample may have been additionally sourced by the Pharusian belt (Fig. 12c) because blueschists
904 were observed in Timétrine (Caby, 2014) and glaucophane bearing eclogites in the Gourma fold and thrust belt
905 north of Gao (Caby et al., 2008). The sample was further characterized by the highest mica content (44 %) among
906 all samples (Fig. 8c) supporting a large dust transport distance.

907

908

909

910

911

912

913

914

915

916

917

918

919

920

921

922

923

924

925

926

927

928 **5. Summary and conclusions**

929 The fluxes, grain-size distributions and the mineral assemblages of the continental trap samples and oceanic
930 sediment trap samples were well comparable to the characteristics of Saharan dust reported for the region. The
931 following main findings were made:

- 932 - A clear seasonal variability in the particle size of mineral dust deposited on land could be observed with
933 generally coarser modal grain sizes during summer compared to winter. The modal particle sizes could be
934 related to the trade wind speed.
- 935 - dust deposited on the continent was predominantly transported from near-by local sources (Mauritania,
936 Western Sahara, Mali), while dust deposited in the marine traps was transported from proximal (Mauritania,
937 Western Sahara, Mali) and distal sources (Senegal and Libya).
- 938 - Some rare characteristic minerals (e.g. ferroglaucophane, rutile, serpentine) could be related to local outcrops
939 in NW Africa

940 To conclude, the particle size and mineralogy of Saharan dust recorded in continental climate archives should be
941 interpreted differently with respect to paleo-environmental conditions compared to marine climate archives; the
942 on-land archive seems to reflect a much more local signal as compared to the regional signal that is recorded in
943 the marine sediments. Given the relationship between particle size and wind strength, we suggest that the particle
944 size in the continental archive in NW Africa may indicate the paleo-wind strength of the trade winds. This is an
945 intuitively logical conclusion, but it has not been demonstrated before so clearly. It should be kept in mind,
946 however, that the wind strength in the sampling location might differ from the wind strength in the source region
947 if the source region is further away. Moreover, the sizes of dust particles present in the source region will influence
948 the grain sizes of deposited dust.

949

950

951

952

953

954

955

956

957

958

959

960

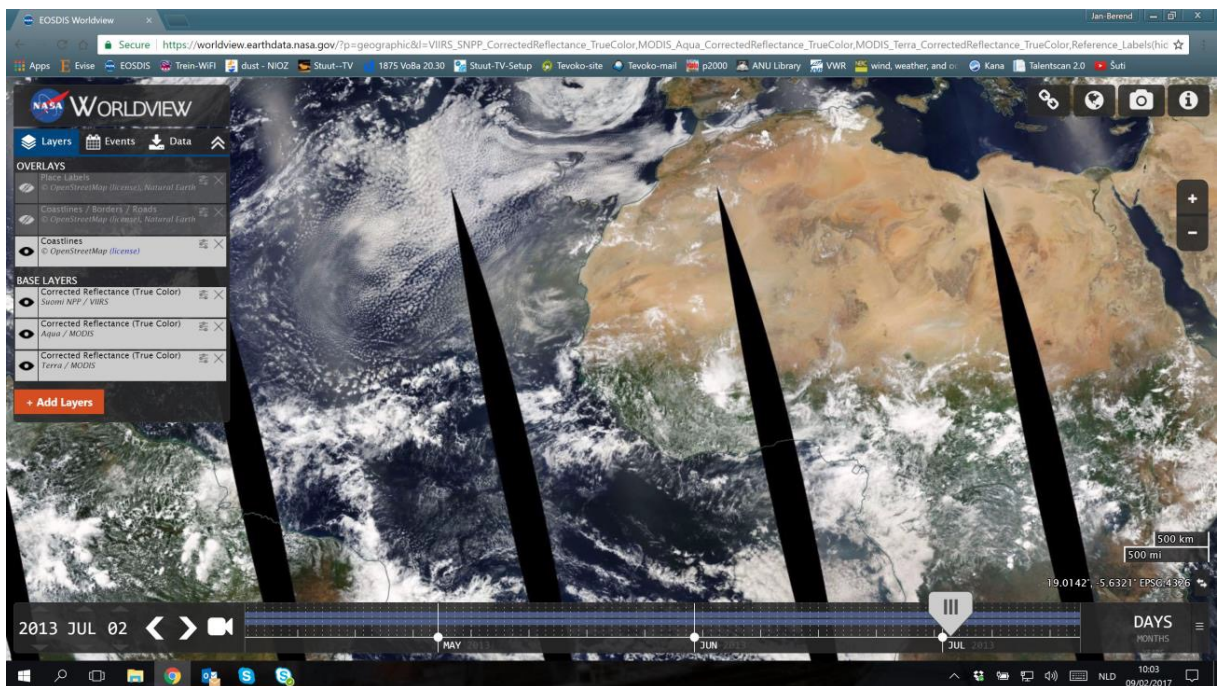
961 6. Appendices

962 A1 Satellite RGB images

963

964 In Fig. A1-4 satellite RGB true colour images are shown of the identified dust storms occurring during the sampling
965 interval of the summer samples of site CBi analysed for dust provenance. On 31 July 2014 only few dust can be
966 observed which overlies the sampling location CBi (Fig. A2). This fits to the observed minor percentage of the
967 mineral ferrylglaucophane (7 %) in the sample which was suggested to be sourced on 31 July 2014 from PSA 3.
968 Zeolite, which was more abundant (22 %) in the dust sample, was therefore most likely derived from PSA 4 due
969 to the major dust storm event occurring on 7 August 2014 (Fig. A3).

970

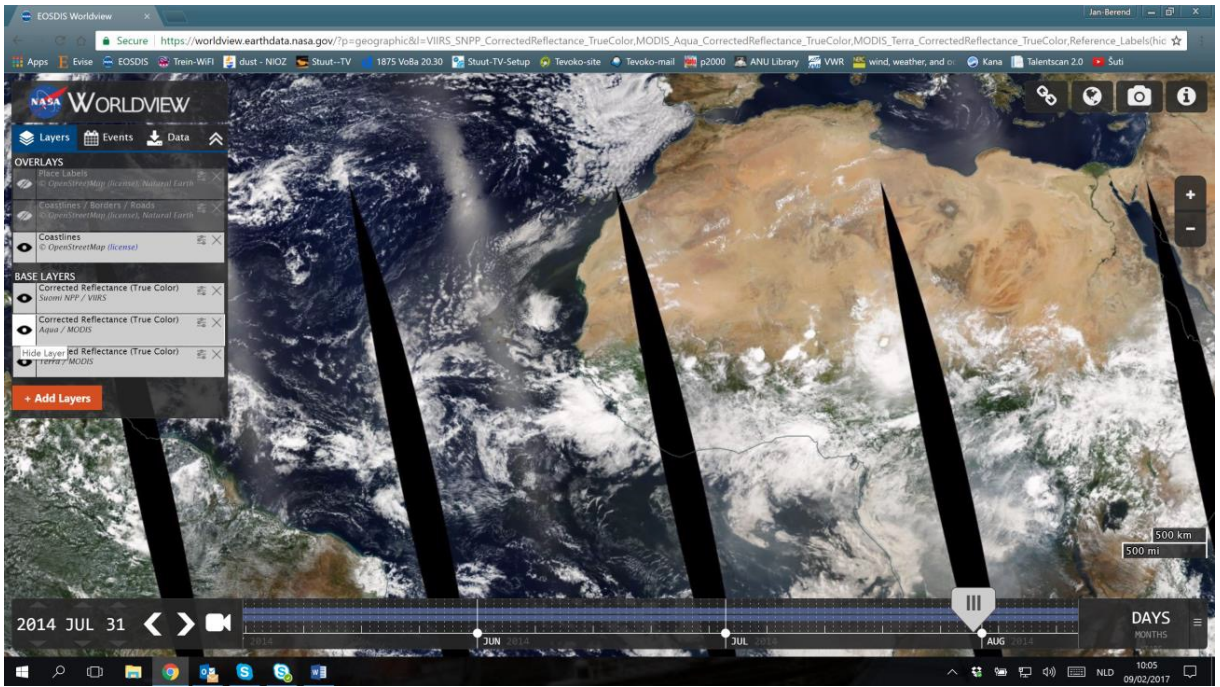


971

972

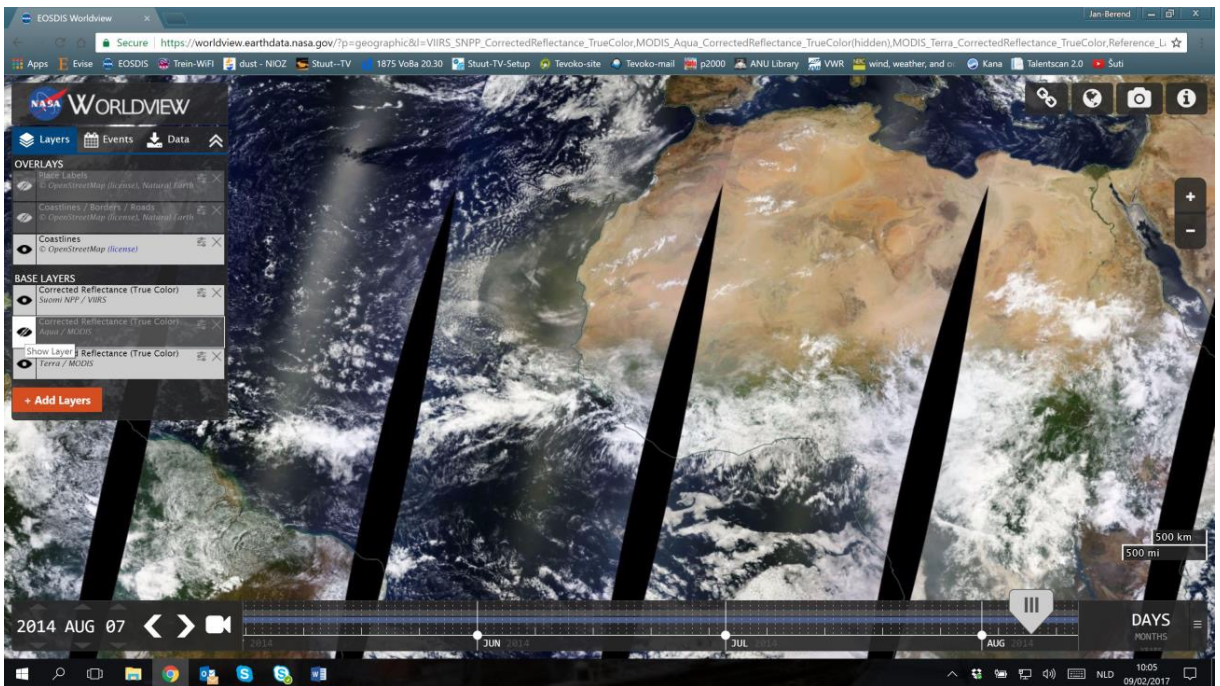
973

Figure A1: Dust storm on 02 July 2013.



974
975

Figure A2: Dust storm on 31 July 2014.



976
977
978

Figure A3: Dust storm on 07 August 2014.

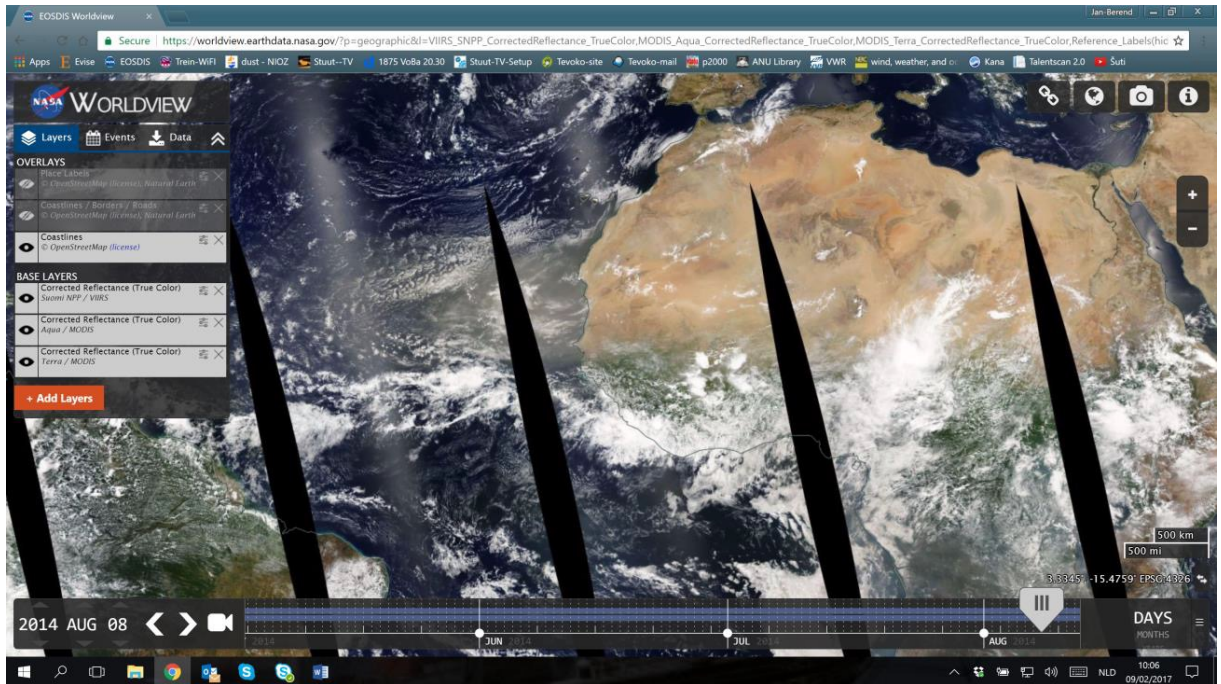


Figure A4: Dust storm on 08 August 2014.

979

980

981

982 **A2 Four day back-trajectories**

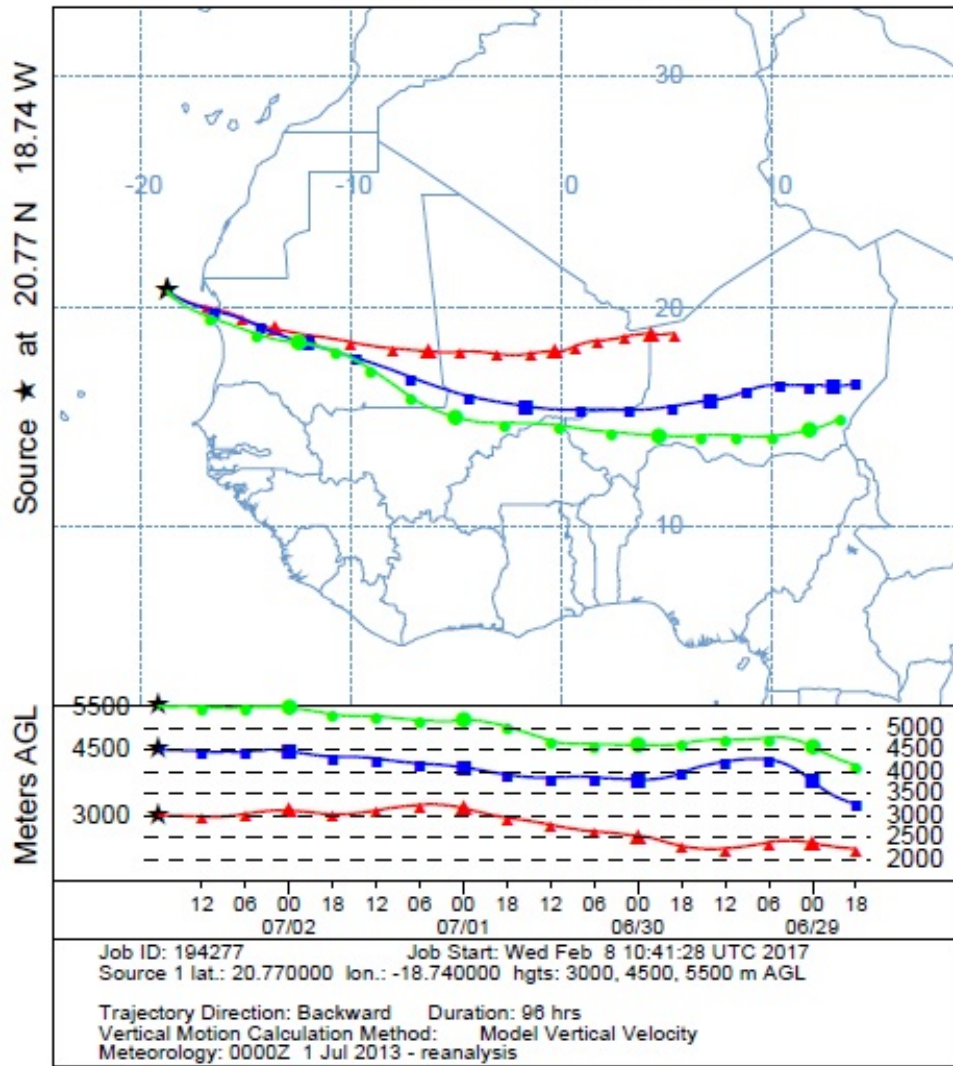
983

984 In Fig. A5-8 the four day back-trajectories are shown calculated at the heights 3000 m, 4500 m and 5500 m ending
 985 at site CBI. These high altitude back-trajectories were calculated for the identified summer days with dust storm
 986 events (shown in Fig A1-4). On the one hand, a height of 4500 m was chosen by Skonieczny et al. (2013) in a dust
 987 provenance study to represent the Saharan air layer (SAL). On the other hand, a height of 5500 m was chosen by
 988 Ratmeyer et al. (1999a) in a dust transport study to represent the SAL. Maximum wind velocities within the SAL
 989 are observed at a height of ~ 3 - 4 km in the area of the Cape Verde Islands during summer according to Carlson
 990 and Prospero (1972). Therefore, we also plotted the back-trajectories at a height of 3000 m. In order to investigate
 991 which air layer should be chosen for provenance studies, the back trajectories of the different heights were
 992 compared.

993 The back-trajectories deviated slightly from each other regarding their direction and length. The back-trajectories
 994 at 3000 m showed the most deviation. Further, the back-trajectories at 4500 m showed the best agreement with the
 995 source areas and the minerals in the samples. Therefore, we chose to use the trajectories at 4500 m for provenance
 996 studies according to Skonieczny et al. (2013).

997

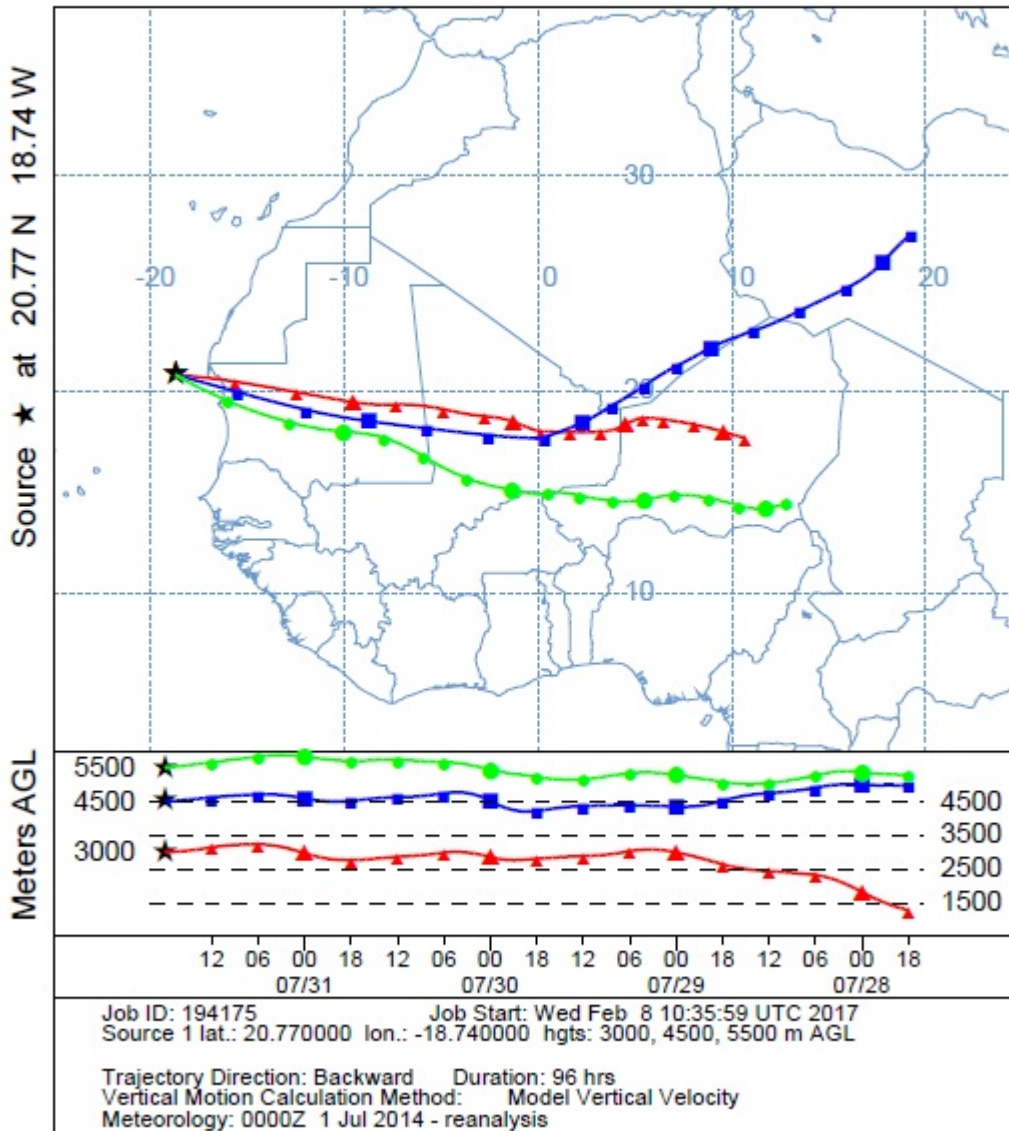
NOAA HYSPLIT MODEL
 Backward trajectories ending at 1800 UTC 02 Jul 13
 CDC1 Meteorological Data



998
 999
 1000

Figure A5: Four day back-trajectories at a height of 3000 m, 4500 m and 5500 m on 02 July 2013.

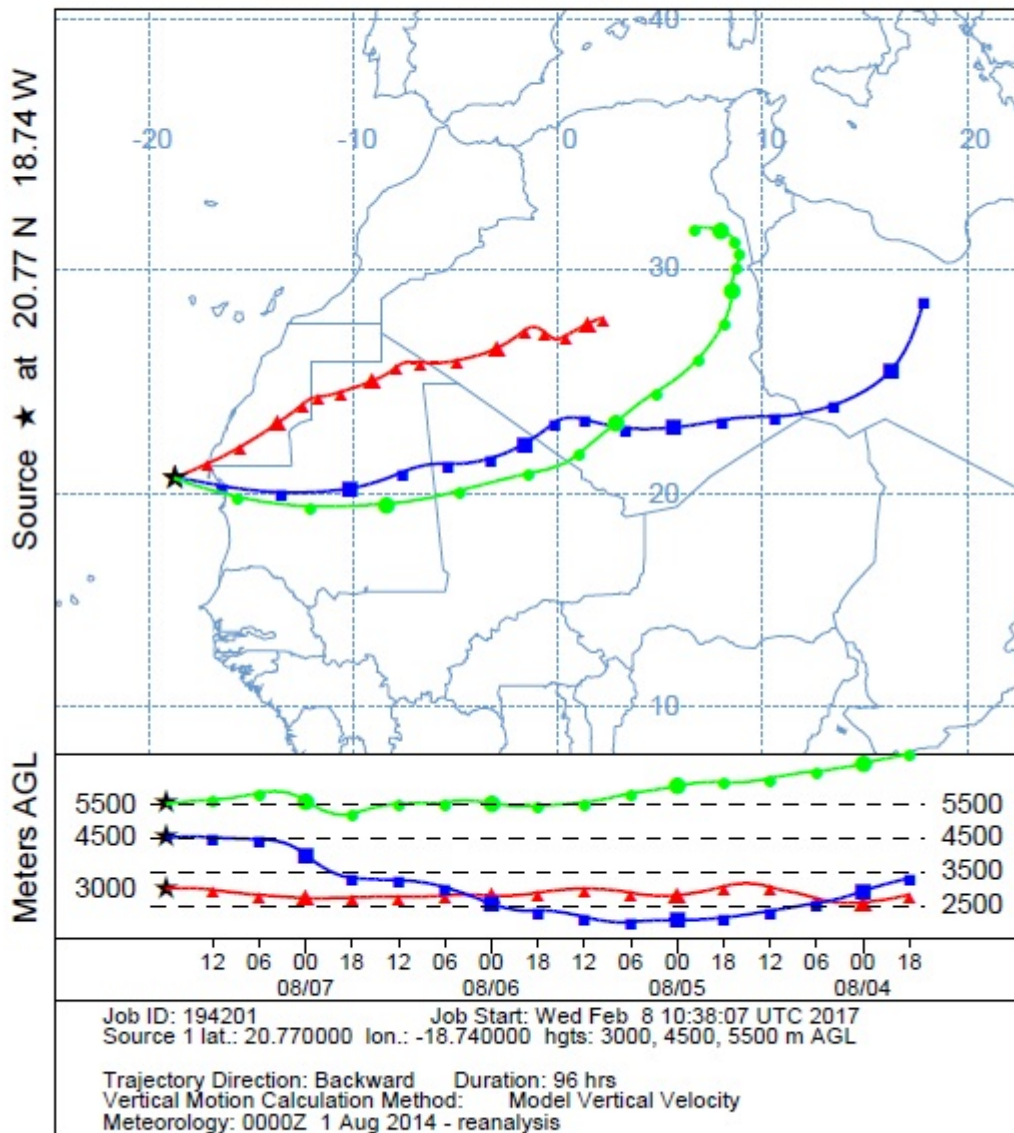
NOAA HYSPLIT MODEL
 Backward trajectories ending at 1800 UTC 31 Jul 14
 CDC1 Meteorological Data



1001
 1002
 1003

Figure A6: Four day back-trajectories at a height of 3000 m, 4500 m and 5500 m on 31 July 2014.

NOAA HYSPLIT MODEL
 Backward trajectories ending at 1800 UTC 07 Aug 14
 CDC1 Meteorological Data

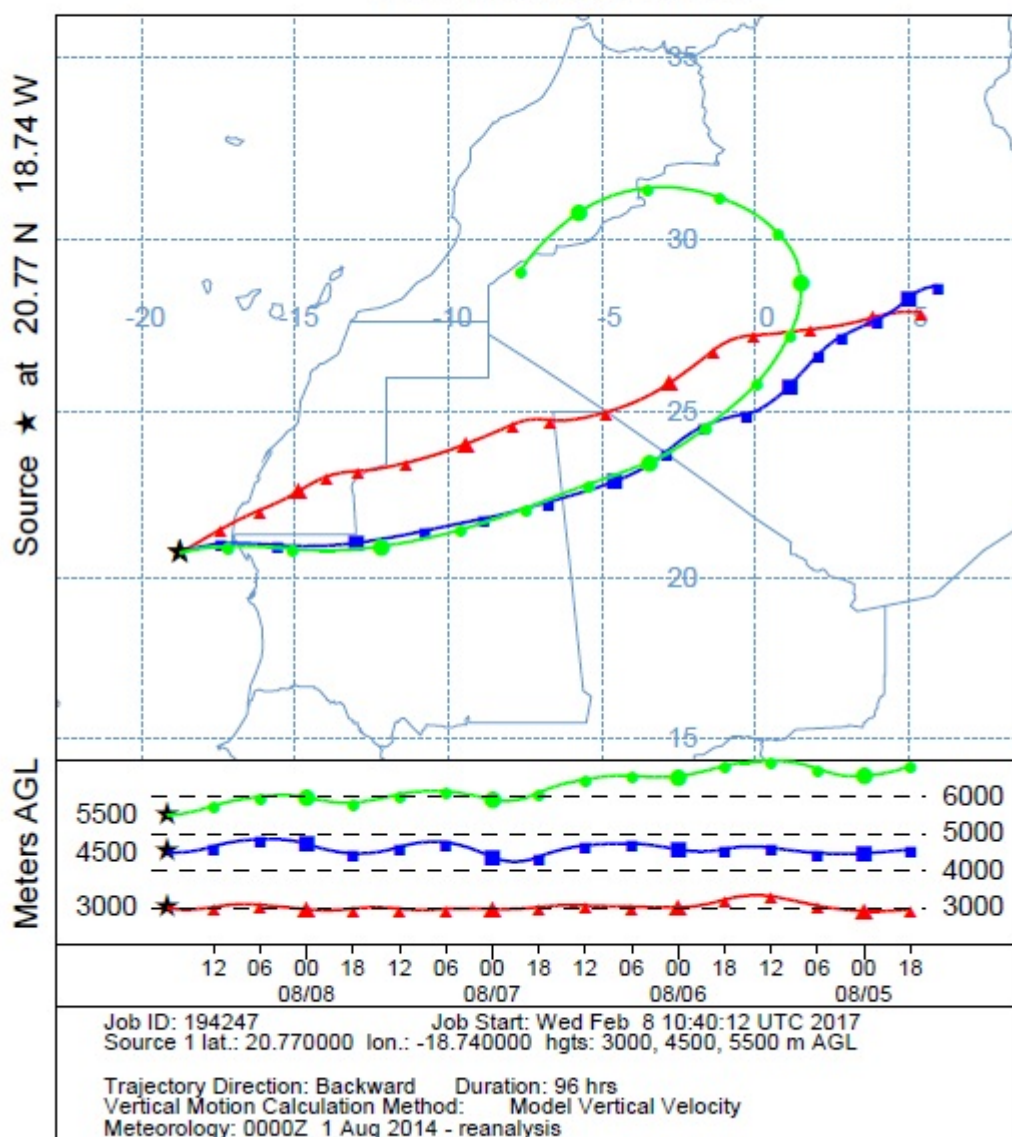


1004

1005

Figure A7: Four day back-trajectories at a height of 3000 m, 4500 m and 5500 m on 07 August 2014.

NOAA HYSPLIT MODEL
 Backward trajectories ending at 1800 UTC 08 Aug 14
 CDC1 Meteorological Data



1006

1007

Figure A8: Four day back-trajectories at a height of 3000 m, 4500 m and 5500 m on 08 August 2014.

1008

1009

7. Supplement link

1010

The data can be accessed on www.pangaea.de.

1011

8. Author contribution

1012

C. Friese carried out the particle size analysis of the sediment trap samples. H. van Hateren carried out the flux

1013

and particle size analysis of the Iwik dust samples. G. Fischer provided the sediment trap samples and supervised

1014

the flux analysis of the sediment trap samples. C. Friese prepared the samples for XRD analysis. C. Vogt carried

1015

out the XRD analysis and was involved in the discussion of the results. J.-B. Stuuut managed the projects through

1016 which dust-collecting buoy ‘Carmen’ was constructed and deployed, supervised the particle-size analysis and the
1017 writing of the manuscript. C. Friese prepared the manuscript with contributions from all co-authors.

1018 **9. Competing interests**

1019 The authors declare that they have no conflict of interest.

1020 **10. Acknowledgements**

1021 We thank the captains, crews and scientific teams of the research cruises with RV Poseidon in 2013 (POS445),
1022 RV Poseidon in 2014 (POS464) and RV Poseidon in 2015 (POS481), during which the sediment traps were
1023 deployed and received. Further, we thank Marco Klann for preparing and splitting the sediment trap samples. Jan-
1024 Berend Stuut acknowledges funding from ERC Grant 311152 DUSTTRAFFIC. Funding is acknowledged from
1025 the German Science Foundation (DFG) through the DFG-Research Center/Cluster of Excellence ‘The Ocean in
1026 the Earth System’. We further thank Prof. Dr. Dierk Hebbeln and Dr. Ute Merkel for helpful and productive
1027 scientific discussions.

1028 **11. References**

- 1029 Abdel-Karim, A.-A. M., Ramadan, E.-N. M., and Embashi, M. R.: Multiphase Alkaline Basalts of Central Al-Haruj Al-
1030 Abyad of Libya: Petrological and Geochemical Aspects, *Journal of Geological Research*, 2013, 12, 10.1155/2013/805451,
1031 2013.
- 1032 Alastuey, A., Querol, X., Castillo, S., Escudero, M., Avila, A., Cuevas, E., Torres, C., Romero, P.-M., Exposito, F., and
1033 García, O.: Characterisation of TSP and PM_{2.5} at Izana and Sta. Cruz de Tenerife (Canary Islands, Spain) during a Saharan
1034 Dust Episode (July 2002), *Atmospheric Environment*, 39, 4715-4728, 2005.
- 1035 Aston, S. R., Chester, R., Johnson, L. R., and Padgham, R. C.: Eolian dust from the lower atmosphere of the eastern Atlantic
1036 and Indian oceans, China Sea and Sea of Japan, *Marine Geology*, 14, 15-28, 1973.
- 1037 Avila, A., Queralt-Mitjans, I., and Alarcon, M.: Mineralogical composition of African dust delivered by red rains over
1038 northeastern Spain, *Journal of Geophysical Research*, 102, 21977-21996, 1997.
- 1039 Bertrand-Sarfati, J., Moussine-Pouchkine, A., Affaton, P., Trompette, R., and Bellion, Y.: Cover sequences of the West
1040 African craton, in: *The West African orogens and circum-Atlantic correlatives*, Springer, 65-82, 1991.
- 1041 Biscaye, P.: Mineralogy and sedimentation of recent Deep-sea clay in the Atlantic Ocean and adjacent seas and oceans., *Geol*
1042 *Soc Am Bull*, 76, 803-832, 1965.
- 1043 Biscaye, P. E.: Mineralogy and sedimentation of the deep-sea sediment fine fraction in the Atlantic Ocean and adjacent seas
1044 and oceans, Ph.D., *Geology*, Yale University, Michigan, 86 pp., 1964.
- 1045 Bloemsmma, M. R., Zabel, M., Stuut, J. B. W., Tjallingii, R., Collins, J. A., and Weltje, G. J.: Modelling the joint variability of
1046 grain size and chemical composition in sediments, *Sedimentary Geology*, 280, 135-148,
1047 <http://dx.doi.org/10.1016/j.sedgeo.2012.04.009>, 2012.

- 1048 Bory, A. J. M., and Newton, P. P.: Transport of airborne lithogenic material down through the water column in two
1049 contrasting regions of the eastern subtropical North Atlantic Ocean, *Global Biogeochem. Cycles*, 14, 297-315,
1050 10.1029/1999gb900098, 2000.
- 1051 Bosse, H.-R., and Gwosdz, W.: Limestone and dolomite resources of Africa, *Geologisches Jahrbuch Reihe D*, 500, 102,
1052 1996.
- 1053 Boullier, A.-M.: The pan-African trans-Saharan belt in the Hoggar shield (Algeria, Mali, Niger): A review, in: *The west*
1054 *African orogens and circum-Atlantic correlatives*, Springer, 85-105, 1991.
- 1055 Caby, R., Buscaïl, F., Dembele, D., Diakite, S., Sacko, S., and Bal, M.: Neoproterozoic garnet-glaucophanites and eclogites:
1056 new insights for subduction metamorphism of the Gourma fold and thrust belt (eastern Mali), *Geological Society, London,*
1057 *Special Publications*, 297, 203-216, 2008.
- 1058 Caby, R.: Nature and evolution of Neoproterozoic ocean-continent transition: Evidence from the passive margin of the West
1059 African craton in NE Mali, *Journal of African Earth Sciences*, 91, 1-11, <http://dx.doi.org/10.1016/j.jafrearsci.2013.11.004>,
1060 2014.
- 1061 Caquineau, S., Gaudichet, A., Gomes, L., and Legrand, M.: Mineralogy of Saharan dust transported over northwestern
1062 tropical Atlantic Ocean in relation to source regions, *Journal of Geophysical Research*, 107, 4251, 2002.
- 1063 Carlson, T. N., and Prospero, J. M.: The Large-Scale Movement of Saharan Air Outbreaks over the Northern Equatorial
1064 Atlantic, *Journal of Applied Meteorology*, 11, 283-297, 1972.
- 1065 Chappell, A., Warren, A., O'Donoghue, A., Robinson, A., Thomas, A., and Bristow, C.: The implications for dust emission
1066 modeling of spatial and vertical variations in horizontal dust flux and particle size in the Bodélé Depression, Northern Chad,
1067 *Journal of Geophysical Research: Atmospheres*, 113, n/a-n/a, 10.1029/2007JD009032, 2008.
- 1068 Chester, R., Elderfield, H., and Griffin, J. J.: Dust transported in the North-east and South-east Trade Winds in the Atlantic
1069 Ocean, *Nature*, 233, 474-476, 10.1038/233474a0, 1971.
- 1070 Chester, R., and Johnson, L. R.: Atmospheric dusts collected off the Atlantic coasts of North Africa and the Iberian
1071 Peninsula, *Marine Geology*, 11, 251-260, 1971a.
- 1072 Chester, R., and Johnson, L. R.: Atmospheric dusts collected off the West African Coast, *Nature*, 229, 105-107, 1971b.
- 1073 Chester, R., Elderfield, H., Griffin, J., Johnson, L., and Padgham, R.: Eolian dust along the eastern margins of the Atlantic
1074 Ocean, *Marine Geology*, 13, 91-105, 1972.
- 1075 Chung, F. H.: Quantitative interpretation of X-ray diffraction patterns of mixtures. I. Matrix-flushing method for quantitative
1076 multicomponent analysis, *Journal of Applied Crystallography*, 7, 519-525, 1974.
- 1077 Cropper, T. E., Hanna, E., and Bigg, G. R.: Spatial and temporal seasonal trends in coastal upwelling off Northwest Africa,
1078 1981–2012, *Deep Sea Research Part I: Oceanographic Research Papers*, 86, 94-111,
1079 <http://dx.doi.org/10.1016/j.dsr.2014.01.007>, 2014.
- 1080 Cvetković, V., Toljić, M., Ammar, N. A., Rundić, L., and Trish, K. B.: Petrogenesis of the eastern part of the Al Haruj basalts
1081 (Libya), *Journal of African Earth Sciences*, 58, 37-50, <http://dx.doi.org/10.1016/j.jafrearsci.2010.01.006>, 2010.

- 1082 Dallmeyer, R. D., and Lécorché, J.-P.: The West African orogens and circum-Atlantic correlatives, Springer Science &
1083 Business Media, 2012.
- 1084 Deer, W. A., Howie, R. A., and Zussman, J.: An introduction to the rock-forming minerals, Longman Scientific & Technical,
1085 1992.
- 1086 Delany, A. C., Claire Delany, A., Parkin, D. W., Griffin, J. J., Goldberg, E. D., and Reimann, B. E. F.: Airborne dust
1087 collected at Barbados, *Geochimica et Cosmochimica Acta*, 31, 885-909, 1967.
- 1088 Diaz, H. F., Carlson, T. N., Prospero, J. M., and Office, E. R. L. W. M. P.: A Study of the Structure and Dynamics of the
1089 Saharan Air Layer Over the Northern Equatorial Atlantic During BOMEX, Nr. 32, Weather Modification Program Office,
1090 Environmental Research Laboratories, 1976.
- 1091 Diester-Haass, L., and Chamley, H.: Neogene paleoenvironment off NW Africa based on sediments from DSDP Leg 14,
1092 *Journal of Sedimentary Research*, 48, 1978.
- 1093 Dobson, M.: An account of the Harmattan, a singular African wind, *Philosophical transactions of the Royal Society of*
1094 *London*, 71, 46-57, 1781.
- 1095 Einsele, G., Herm, D., and Schwarz, H. U.: Sea level fluctuation during the past 6000 yr at the coast of Mauritania,
1096 *Quaternary Research*, 4, 282-289, [http://dx.doi.org/10.1016/0033-5894\(74\)90017-9](http://dx.doi.org/10.1016/0033-5894(74)90017-9), 1974.
- 1097 El Makkrouf, A. A.: Tectonic interpretation of Jabal Eghei area and its regional application to Tibesti orogenic belt, south
1098 central Libya (S.P.L.A.J.), *Journal of African Earth Sciences (and the Middle East)*, 7, 945-967,
1099 [http://dx.doi.org/10.1016/0899-5362\(88\)90009-7](http://dx.doi.org/10.1016/0899-5362(88)90009-7), 1988.
- 1100 Filipsson, H. L., Romero, O. E., Stuut, J.-B. W., and Donner, B.: Relationships between primary productivity and bottom-
1101 water oxygenation off northwest Africa during the last deglaciation, *Journal of Quaternary Science*, 26, 448-456,
1102 DOI:10.1002/jqs.1473, 2011.
- 1103 Fischer, G., and Wefer, G.: Sampling, Preparation and Analysis of Marine Particulate Matter, *Geoph Monog Series*, 63, 391-
1104 397, 1991.
- 1105 Fischer, G., and Karakas, G.: Sinking rates and ballast composition of particles in the Atlantic Ocean: implications for the
1106 organic carbon fluxes to the deep ocean, *Biogeosciences*, 6, 85-102, 2009.
- 1107 Fischer, G., Ba, M., Dehning, K., Hefter, J., Iversen, M., Klann, M., Nowald, N., Ploug, H., Ruhland, G., and Witte, Y.:
1108 Report and preliminary results of R/V POSEIDON cruise POS445. Las Palmas–Las Palmas, 19.01. 2013–01.02. 2013, 2013.
- 1109 Fischer, G., Dehning, K., Dia, A., Füssel, J., Hefter, J., Iversen, M., Klann, M., Nowald, N., Olbrich, M., and Ruhland, G.:
1110 Report and preliminary results of RV POSEIDON cruise POS464, Las Palmas (Canary Islands)-Las Palmas (Canary Islands),
1111 03.02. 2014-18.02. 2014, 2014.
- 1112 Fischer, G., Dia, A., Iversen, M., Klann, M., Nowald, N., Markussen, T., Meckel, S., Ruhland, G., Van der Jagt, H., and
1113 Waldmann, C.: Report and preliminary results of R/V POSEIDON cruise POS481, Las Palmas (Canary Islands)-Las Palmas
1114 (Canary Islands), 15.03. 2015-03.03. 2015, 2015a.

- 1115 Fischer, G., Romero, O., Merkel, U., Donner, B., Iversen, M., Nowald, N., Ratmeyer, V., Ruhland, G., Klann, M., and Wefer,
1116 G.: Deep ocean mass fluxes in the coastal upwelling off Mauritania from 1988 to 2012: variability on seasonal to decadal
1117 timescales, *Biogeosciences Discussions*, 12, 2015b.
- 1118 Formenti, P., Rajot, J. L., Desboeufs, K., Caquineau, S., Chevaillier, S., Nava, S., Gaudichet, A., Journet, E., Triquet, S.,
1119 Alfaro, S., Chiari, M., Haywood, J., Coe, H., and Highwood, E.: Regional variability of the composition of mineral dust from
1120 western Africa: Results from the AMMA SOP0/DABEX and DODO field campaigns, *Journal of Geophysical Research:*
1121 *Atmospheres*, 113, n/a-n/a, [10.1029/2008JD009903](https://doi.org/10.1029/2008JD009903), 2008.
- 1122 Friese, C. A., van der Does, M., Merkel, U., Iversen, M. H., Fischer, G., and Stuut, J.-B. W.: Environmental factors
1123 controlling the seasonal variability in particle size distribution of modern Saharan dust deposited off Cape Blanc, *Aeolian*
1124 *Research*, 22, 165-179, <http://dx.doi.org/10.1016/j.aeolia.2016.04.005>, 2016.
- 1125 Fütterer, D.: Sedimentation am NW-afrikanischen Kontinentalrand: Quantitative Zusammensetzung und Verteilung der
1126 Siltfraktion in den Oberflächensedimenten, *Meteor-Forschungsergebnisse, C*, 15-60, 1980.
- 1127 Gac, J. Y., and Kane, A.: Le Fleuve Sénégal: I. Bilan hydrologique et flux continentaux de matières particulaires a
1128 l'embouchure, *Sci. Géol. Bull.*, 39, 99-130, 1986.
- 1129 García-Romero, E., Suárez, M., Santarén, J., and Alvarez, A.: Crystallochemical Characterization of the Palygorskite and
1130 Sepiolite from the Allou Kagne Deposit, Senegal, *Clays and Clay Minerals*, 55, 606-617, [10.1346/CCMN.2007.0550608](https://doi.org/10.1346/CCMN.2007.0550608),
1131 2007.
- 1132 Gillies, J. A., Nickling, W. G., and McTainsh, G. H.: Dust concentrations and particle-size characteristics of an intense dust
1133 haze event: inland delta region, Mali, West Africa, *Atmospheric Environment*, 30, 1081-1090, 1996.
- 1134 Glaccum, R. A., and Prospero, J. M.: Saharan aerosols over the tropical North Atlantic - mineralogy, *Marine Geology*, 37,
1135 295-321, 1980.
- 1136 Goossens, D., and Offer, Z. Y.: Wind tunnel and field calibration of six aeolian dust samplers, *Atmospheric Environment*, 34,
1137 1043-1057, [10.1016/s1352-2310\(99\)00376-3](https://doi.org/10.1016/s1352-2310(99)00376-3), 2000.
- 1138 Goossens, D.: Relationships between horizontal transport flux and vertical deposition flux during dry deposition of
1139 atmospheric dust particles, *Journal of Geophysical Research: Earth Surface*, 113, n/a-n/a, [10.1029/2007JF000775](https://doi.org/10.1029/2007JF000775), 2008.
- 1140 Griffin, J. J., Windom, H., and Goldberg, E. D.: The distribution of clay minerals in the World Ocean, *Deep Sea Research*
1141 *and Oceanographic Abstracts*, 15, 433-459, [http://dx.doi.org/10.1016/0011-7471\(68\)90051-X](http://dx.doi.org/10.1016/0011-7471(68)90051-X), 1968.
- 1142 Haywood, J., and Boucher, O.: Estimates of the direct and indirect radiative forcing due to tropospheric aerosols: A review,
1143 *Rev Geophys*, 38, 513-543, [Doi 10.1029/1999rg000078](https://doi.org/10.1029/1999rg000078), 2000.
- 1144 Holz, C., Stuut, J.-B. W., and Henrich, R.: Terrigenous sedimentation processes along the continental margin off NW-Africa:
1145 implications from grain-size analyses of surface sediments, *Sedimentology*, 51, 1145-1154, [.1111/j.1365-3091.2004.00665.x](https://doi.org/10.1111/j.1365-3091.2004.00665.x),
1146 2004.
- 1147 Holz, C., Stuut, J.-B. W., Henrich, R., and Meggers, H.: Variability in terrigenous sedimentation processes off northwest
1148 Africa and its relation to climate changes: Inferences from grain-size distributions of a Holocene marine sediment record,
1149 *Sedimentary Geology*, 202, 499-508, [10.1016/j.sedgeo.2007.03.015](https://doi.org/10.1016/j.sedgeo.2007.03.015), 2007.

- 1150 Iversen, M. H., Nowald, N., Ploug, H., Jackson, G. A., and Fischer, G.: High resolution profiles of vertical particulate organic
1151 matter export off Cape Blanc, Mauritania: Degradation processes and ballasting effects, *Deep Sea Research Part I:*
1152 *Oceanographic Research Papers*, 57, 771-784, DOI: 10.1016/j.dsr.2010.03.007, 2010.
- 1153 Iversen, M. H., and Ploug, H.: Ballast minerals and the sinking carbon flux in the ocean: carbon-specific respiration rates and
1154 sinking velocities of macroscopic organic aggregates (marine snow), *Biogeosciences Discuss.*, 7, 3335-3364, 10.5194/bgd-7-
1155 3335-2010, 2010.
- 1156 Iversen, M. H., and Robert, M. L.: Ballasting effects of smectite on aggregate formation and export from a natural plankton
1157 community, *Marine Chemistry*, 175, 18-27, <http://dx.doi.org/10.1016/j.marchem.2015.04.009>, 2015.
- 1158 Jickells, T. D., An, Z. S., Andersen, K. K., Baker, A. R., Bergametti, G., Brooks, N., Cao, J. J., Boyd, P. W., Duce, R. A.,
1159 Hunter, K. A., Kawahata, H., Kubilay, N., laRoche, J., Liss, P. S., Mahowald, N., Prospero, J. M., Ridgwell, A. J., Tegen, I.,
1160 and Torres, R.: Global Iron Connections Between Desert Dust, Ocean Biogeochemistry, and Climate, *Science*, 308, 67-71,
1161 2005.
- 1162 Johnson, L. R.: Mineralogical dispersal patterns of North Atlantic deep-sea sediments with particular reference to eolian
1163 dusts, *Marine Geology*, 29, 335-345, [http://dx.doi.org/10.1016/0025-3227\(79\)90115-4](http://dx.doi.org/10.1016/0025-3227(79)90115-4), 1979.
- 1164 Journet, E., Balkanski, Y., and Harrison, S. P.: A new data set of soil mineralogy for dust-cycle modeling, *Atmos. Chem.*
1165 *Phys.*, 14, 3801-3816, 10.5194/acp-14-3801-2014, 2014.
- 1166 Kandler, K., Schütz, L., Deutscher, C., Ebert, M., Hofmann, H., Jäckel, S., Jaenicke, R., Knippertz, P., Lieke, K., Massling,
1167 A., Petzold, A., Schladitz, A., Weinzierl, B., Wiedensohler, A., Zorn, S., and Weinbruch, S.: Size distribution, mass
1168 concentration, chemical and mineralogical composition and derived optical parameters of the boundary layer aerosol at
1169 Tinfou, Morocco, during SAMUM 2006, *Tellus B*, 61, 32-50, 10.1111/j.1600-0889.2008.00385.x, 2009.
- 1170 Khiri, F., Ezaidi, A., and Kabbachi, K.: Dust deposits in Souss-Massa basin, South-West of Morocco: granulometrical,
1171 mineralogical and geochemical characterisation, *Journal of African Earth Sciences*, 39, 459-464, 2004.
- 1172 Knippertz, P., and Todd, M. C.: Mineral dust aerosols over the Sahara: Meteorological controls on emission and transport and
1173 implications for modeling, *Rev Geophys*, 50, n/a-n/a, 10.1029/2011RG000362, 2012.
- 1174 Knippertz, P., and Stuut, J.-B. W.: *Mineral dust a key player in the Earth system*, Springer, Dordrecht, 2014.
- 1175 Koch, J., and Renno, N. O.: The role of convective plumes and vortices on the global aerosol budget, *Geophysical Research*
1176 *Letters*, 32, n/a-n/a, 10.1029/2005GL023420, 2005.
- 1177 Kogbe, C. A.: Geology of the upper cretaceous and tertiary sediments of the Nigerian sector of the Iullemeden Basin (West-
1178 Africa), *Geol Rundsch*, 62, 197-211, 10.1007/bf01826827, 1973.
- 1179 Koopmann, B.: Sedimentation von Saharastaub im subtropischen Nordatlantik während der letzten 25.000 Jahre, *Meteor*
1180 *Forschungsergebnisse C*, 35, 23-59, 1981.
- 1181 Korte, L. F., Brummer, G. J., van der Does, M., Guerreiro, C. V., Hennekam, R., van Hateren, J. A., Jong, D., Munday, C. I.,
1182 Schouten, S., and Stuut, J. B. W.: Downward particle fluxes of biogenic matter and Saharan dust across the equatorial North
1183 Atlantic, *Atmos. Chem. Phys.*, 17, 6023-6040, 10.5194/acp-17-6023-2017, 2017.

- 1184 Lancaster, N.: 11.12 Sand Seas and Dune Fields A2 - Shroder, John F, in: *Treatise on Geomorphology*, Academic Press, San
1185 Diego, 219-245, 2013.
- 1186 Lange, H.: Herkunft und Verteilung von Oberflächensedimenten des westafrikanischen Schelfs und Kontinentalhanges. *‘*,
1187 “Meteor” *Forschungsergeb*, 22, 61-84, 1975.
- 1188 Lange, H.: Distribution of Chlorite and Kaolinite in Eastern Atlantic Sediments Off North-Africa, *Sedimentology*, 29, 427-
1189 431, DOI 10.1111/j.1365-3091.1982.tb01805.x, 1982.
- 1190 Lau, K. M., and Kim, K. M.: Cooling of the Atlantic by Saharan dust, *Geophys. Res. Lett.*, 34, 10.1029/2007GL031538,
1191 2007.
- 1192 Martin, J. H.: Glacial-interglacial CO₂ change: the iron hypothesis, *Paleoceanography*, 5, 1-13, 1990.
- 1193 Martin, J. H., Gordon, R. M., and Fitzwater, S. E.: The case for iron, *Limnology & Oceanography*, 36, 1793-1802, 1991.
- 1194 McTainsh, G. H., Nickling, W. G., and Lynch, A. W.: Dust deposition and particle size in Mali, West Africa, *Catena*, 29,
1195 307-322, 1997.
- 1196 Mendez, M. J., Funk, R., and Buschiazzo, D. E.: Field wind erosion measurements with Big Spring Number Eight (BSNE)
1197 and Modified Wilson and Cook (MWAC) samplers, *Geomorphology*, 129, 43-48, 10.1016/j.geomorph.2011.01.011, 2011.
- 1198 Meunier, T., Barton, E. D., Barreiro, B., and Torres, R.: Upwelling filaments off Cap Blanc: Interaction of the NW African
1199 upwelling current and the Cape Verde frontal zone eddy field?, *Journal of Geophysical Research: Oceans*, 117, n/a-n/a,
1200 10.1029/2012JC007905, 2012.
- 1201 Meyer, I., Davies, G. R., Vogt, C., Kuhlmann, H., and Stuu, J.-B. W.: Changing rainfall patterns in NW Africa since the
1202 Younger Dryas, *Aeolian Research*, 10, 111-123, <http://dx.doi.org/10.1016/j.aeolia.2013.03.003>, 2013.
- 1203 Mittelstaedt, E.: The ocean boundary along the northwest African coast: Circulation and oceanographic properties at the sea
1204 surface, *Progress In Oceanography*, 26, 307-355, 10.1016/0079-6611(91)90011-A, 1991.
- 1205 Moore, D. M., and Reynolds, R. C.: *X-ray Diffraction and the Identification and Analysis of Clay Minerals*, Oxford
1206 university press Oxford, 1989.
- 1207 Moreno, T., Querol, X., Castillo, S., Alastuey, A., Cuevas, E., Herrmann, L., Mounkaila, M., Elvira, J., and Gibbons, W.:
1208 Geochemical variations in aeolian mineral particles from the Sahara-Sahel Dust Corridor, *Chemosphere*, 65, 261-270, 2006.
- 1209 Mulitza, S., Heslop, D., Pittauerova, D., Fischer, H. W., Meyer, I., Stuu, J.-B., Zabel, M., Mollenhauer, G., Collins, J. A.,
1210 Kuhnert, H., and Schulz, M.: Increase in African dust flux at the onset of commercial agriculture in the Sahel region, *Nature*,
1211 466, 226-228, 10.1038/nature09213, 2010.
- 1212 National Geospatial-Intelligence Agency: *North Atlantic, Baltic Sea, North Sea and Mediterranean Sea*, 4 ed., Sailing
1213 directions (planning guide), ProStar Publications, 2006.
- 1214 Nicholson, S. E.: A revised picture of the structure of the "monsoon" and land ITCZ over West Africa, *Climate Dynamics*,
1215 32, 1155-1171, DOI 10.1007/s00382-008-0514-3, 2009.

- 1216 Nizou, J., Hanebuth, T. J. J., and Vogt, C.: Deciphering signals of late Holocene fluvial and aeolian supply from a shelf
1217 sediment depocentre off Senegal (north-west Africa), *Journal of Quaternary Science*, n/a-n/a, 10.1002/jqs.1467, 2011.
- 1218 Piqué, A.: *Geology of northwest Africa*, Gebrüder Borntraeger, 2001.
- 1219 Ploug, H., Iversen, M. H., and Fischer, G.: Ballast, sinking velocity, and apparent diffusivity within marine snow and
1220 zooplankton fecal pellets: Implications for substrate turnover by attached bacteria, *Limnology and Oceanography*, 53, 1878-
1221 1886, 2008a.
- 1222 Ploug, H., Iversen, M. H., Koski, M., and Buitenhuis, E. T.: Production, oxygen respiration rates, and sinking velocity of
1223 copepod fecal pellets: Direct measurements of ballasting by opal and calcite, *Limnology and Oceanography*, 53, 469-476,
1224 DOI 10.4319/lo.2008.53.2.0469, 2008b.
- 1225 Proske, U., Hanebuth, T. J. J., Meggers, H., and Leroy, S. A. G.: Tidal flat sedimentation during the last millennium in the
1226 northern area of Tidra Island, Banc d'Arguin, Mauritania, *Journal of African Earth Sciences*, 50, 37-48,
1227 <http://dx.doi.org/10.1016/j.jafrearsci.2007.09.002>, 2008.
- 1228 Prospero, J. M., and Carlson, T. N.: Radon-222 in North Atlantic Trade Winds . Its Relationship to Dust Transport from
1229 Africa, *Science*, 167, 974-&, Doi 10.1126/Science.167.3920.974, 1970.
- 1230 Prospero, J. M., and Carlson, T. N.: Vertical and areal distribution of Saharan dust over the western equatorial north Atlantic
1231 Ocean, *Journal of Geophysical Research*, 77, 5255-5265, 10.1029/JC077i027p05255, 1972.
- 1232 Prospero, J. M., Ginoux, P., Torres, O., Nicholson, S. E., and Gill, T. E.: Environmental characterization of global sources of
1233 atmospheric soil dust identified with the Nimbus 7 total ozone mapping spectrometer (TOMS) absorbing aerosol product,
1234 *Rev Geophys*, 40, 1-31, 2002.
- 1235 Pye, K.: The nature, origin and accumulation of loess, *Quaternary Science Reviews*, 14, 653-667, 1995.
- 1236 Radczewski, O. E.: Eolian deposits in marine sediments, 1939.
- 1237 Rateev, M. A., Gorbunova, Z. N., Lisitzyn, A. P., and Nosov, G. L.: THE DISTRIBUTION OF CLAY MINERALS IN THE
1238 OCEANS, *Sedimentology*, 13, 21-43, 10.1111/j.1365-3091.1969.tb01119.x, 1969.
- 1239 Ratmeyer, V., Balzer, W., Bergametti, G., Chiapello, I., Fischer, G., and Wyputta, U.: Seasonal impact of mineral dust on
1240 deep-ocean particle flux in the eastern subtropical Atlantic Ocean, *Marine Geology*, 159, 241-252, 1999a.
- 1241 Ratmeyer, V., Fischer, G., and Wefer, G.: Lithogenic particle fluxes and grain size distributions in the deep ocean off
1242 northwest Africa: Implications for seasonal changes of aeolian dust input and downward transport, *Deep Sea Research Part I:
1243 Oceanographic Research Papers*, 46, 1289-1337, 1999b.
- 1244 Rea, D. K.: The paleoclimatic record provided by eolian deposition in the deep sea: the geologic history of wind, *Rev
1245 Geophys*, 32, 159-195, 1994.
- 1246 Santamarina, J., and Cho, G.: Soil behaviour: The role of particle shape, *Advances in geotechnical engineering: The
1247 skempton conference, 2004*, 604-617,

- 1248 Scheuven, D., Schütz, L., Kandler, K., Ebert, M., and Weinbruch, S.: Bulk composition of northern African dust and its
1249 source sediments — A compilation, *Earth-Science Reviews*, 116, 170-194, <http://dx.doi.org/10.1016/j.earscirev.2012.08.005>,
1250 2013.
- 1251 Schlüter, T.: *Geological atlas of Africa*, Springer, 2008.
- 1252 Schofield, D., Horstwood, M., Pitfield, P., Crowley, Q., Wilkinson, A., and Sidaty, H. C. O.: Timing and kinematics of
1253 Eburnean tectonics in the central Reguibat Shield, Mauritania, *Journal of the Geological Society*, 163, 549-560, 2006.
- 1254 Schuster, M., Düringer, P., Ghienne, J.-F., Roquin, C., Sepulchre, P., Moussa, A., Lebatard, A.-E., Mackaye, H. T., Likius,
1255 A., Vignaud, P., and Brunet, M.: Chad Basin: Paleoenvironments of the Sahara since the Late Miocene, *Comptes Rendus*
1256 *Geoscience*, 341, 603-611, <http://dx.doi.org/10.1016/j.crte.2009.04.001>, 2009.
- 1257 Schütz, L., and Sebert, M.: Mineral aerosols and source identification, *Journal of Aerosol Science*, 18, 1-10,
1258 [http://dx.doi.org/10.1016/0021-8502\(87\)90002-4](http://dx.doi.org/10.1016/0021-8502(87)90002-4), 1987.
- 1259 Selley, R. C.: Chapter 3 The sirte basin of libya, in: *Sedimentary Basins of the World*, edited by: Selley, R. C., Elsevier, 27-
1260 37, 1997a.
- 1261 Selley, R. C.: Chapter 1 The sedimentary basins of northwest africa: stratigraphy and sedimentation, in: *Sedimentary Basins*
1262 *of the World*, edited by: Selley, R. C., Elsevier, 3-16, 1997b.
- 1263 Selley, R. C.: Chapter 2 The basins of northwest africa: Structural evolution, in: *Sedimentary Basins of the World*, edited by:
1264 Selley, R. C., Elsevier, 17-26, 1997c.
- 1265 Skonieczny, C., Bory, A., Bout-Roumazeilles, V., Abouchami, W., Galer, S. J. G., Crosta, X., Stuut, J. B., Meyer, I.,
1266 Chiapello, I., Podvin, T., Chatenet, B., Diallo, A., and Ndiaye, T.: The 7-13 March 2006 major Saharan outbreak: Multiproxy
1267 characterization of mineral dust deposited on the West African margin, *J. Geophys. Res.*, 116, D18210,
1268 [10.1029/2011jd016173](https://doi.org/10.1029/2011jd016173), 2011.
- 1269 Skonieczny, C., Bory, A., Bout-Roumazeilles, V., Abouchami, W., Galer, S. J. G., Crosta, X., Diallo, A., and Ndiaye, T.: A
1270 three-year time series of mineral dust deposits on the West African margin: Sedimentological and geochemical signatures and
1271 implications for interpretation of marine paleo-dust records, *Earth and Planetary Science Letters*, 364, 145-156,
1272 <http://dx.doi.org/10.1016/j.epsl.2012.12.039>, 2013.
- 1273 Stein, A. F., Draxler, R. R., Rolph, G. D., Stunder, B. J. B., Cohen, M. D., and Ngan, F.: NOAA's HYSPLIT Atmospheric
1274 Transport and Dispersion Modeling System, *Bulletin of the American Meteorological Society*, 96, 2059-2077, [10.1175/bams-](https://doi.org/10.1175/bams-d-14-00110.1)
1275 [d-14-00110.1](https://doi.org/10.1175/bams-d-14-00110.1), 2015.
- 1276 Stein, R.: Late neogene changes of paleoclimate and paleoproductivity off northwest africa (D.S.D.P. Site 397),
1277 *Palaeogeography, Palaeoclimatology, Palaeoecology*, 49, 47-59, [http://dx.doi.org/10.1016/0031-0182\(85\)90004-5](http://dx.doi.org/10.1016/0031-0182(85)90004-5), 1985.
- 1278 Stuut, J.-B. W.: Late Quaternary Southwestern African terrestrial-climate signals in the marine record of Walvis Ridge, SE
1279 Atlantic Ocean, *Faculty of Earth Sciences, Utrecht University, Utrecht*, 128 pp., 2001.
- 1280 Stuut, J.-B. W., Zabel, M., Ratmeyer, V., Helmke, P., Schefuß, E., Lavik, G., and Schneider, R. R.: Provenance of present-
1281 day eolian dust collected off NW Africa, *Journal of Geophysical Research*, 110, [10.1029/2004JD005161](https://doi.org/10.1029/2004JD005161), 2005.

- 1282 Stuut, J.-B. W., Smalley, I., and O'Hara-Dhand, K.: Aeolian dust in Europe: African sources and European deposits,
1283 *Quaternary International*, 198, 234-245, 10.1016/j.quaint.2008.10.007, 2009.
- 1284 Stuut, J.-B. W., Bakker, M., Friese, C., Koster, B., Visser, J.-D. d., and Witte, Y.: Cruise Report and preliminary results -
1285 DUSTTRAFFIC: Transatlantic fluxes of Saharan dust - Cruise No. 64PE392 - 19 – 27 August 2014 Las Palmas de Gran
1286 Canaria (Spain) – Mindelo, Sao Vicente (Cape Verdian Islands), 2015.
- 1287 Ternon, E., Guieu, C., Loÿe-Pilot, M. D., Leblond, N., Bosc, E., Gasser, B., Miquel, J. C., and Martín, J.: The impact of
1288 Saharan dust on the particulate export in the water column of the North Western Mediterranean Sea, *Biogeosciences*, 7, 809-
1289 826, 10.5194/bg-7-809-2010, 2010.
- 1290 Tjallingii, R., Claussen, M., Stuut, J.-B. W., Fohlmeister, J., Jahn, A., Bickert, T., Lamy, F., and Rohl, U.: Coherent high- and
1291 low-latitude control of the northwest African hydrological balance, *Nature Geoscience*, 1, 670-675, 10.1038/ngeo289, 2008.
- 1292 Tsoar, H., and Pye, K.: Dust transport and the question of desert loess formation, *Sedimentology*, 34, 139-153, 1987.
- 1293 Tucker, M. E., and Tucker, M.: *Techniques in sedimentology*, 552.5. 08 TEC, 1988.
- 1294 Van Camp, L., Nykjaer, L., Mittelstaedt, E., and Schlittenhardt, P.: Upwelling and boundary circulation off Northwest Africa
1295 as depicted by infrared and visible satellite observations, *Progress in Oceanography*, 26, 357-402,
1296 [http://dx.doi.org/10.1016/0079-6611\(91\)90012-B](http://dx.doi.org/10.1016/0079-6611(91)90012-B), 1991.
- 1297 Van der Does, M., Korte, L. F., Munday, C. I., Brummer, G. J. A., and Stuut, J. B. W.: Particle size traces modern Saharan
1298 dust transport and deposition across the equatorial North Atlantic, *Atmos. Chem. Phys.*, 16, 13697-13710, 10.5194/acp-16-
1299 13697-2016, 2016.
- 1300 Verati, C., Bertrand, H., and Féraud, G.: The farthest record of the Central Atlantic Magmatic Province into West Africa
1301 craton: Precise ⁴⁰Ar/³⁹Ar dating and geochemistry of Taoudenni basin intrusives (northern Mali), *Earth and Planetary
1302 Science Letters*, 235, 391-407, <http://dx.doi.org/10.1016/j.epsl.2005.04.012>, 2005.
- 1303 Villeneuve, M.: Paleozoic basins in West Africa and the Mauritanide thrust belt, *Journal of African Earth Sciences*, 43, 166-
1304 195, <http://dx.doi.org/10.1016/j.jafrearsci.2005.07.012>, 2005.
- 1305 Vogt, C., Lauterjung, J., and Fischer, R. X.: Investigation of the Clay Fraction (< 2 µm) of the Clay Minerals Society
1306 Reference Clays, *Clays and Clay Minerals*, 50, 388-400, 2002.
- 1307 Wilson, S., and Cooke, R.: Wind erosion, Soil erosion, 217251, 1980.
- 1308 Wissmann, G.: Stratigraphy and structural features of the continental margin basin of Senegal and Mauritania, in: *Geology of
1309 the Northwest African continental margin*, Springer, 160-181, 1982.
- 1310 Yoshioka, M., Mahowald, N. M., Conley, A. J., Collins, W. D., Fillmore, D. W., Zender, C. S., and Coleman, D. B.: Impact
1311 of Desert Dust Radiative Forcing on Sahel Precipitation: Relative Importance of Dust Compared to Sea Surface Temperature
1312 Variations, Vegetation Changes, and Greenhouse Gas Warming, *Journal of Climate*, 20, 1445-1467,
1313 doi:10.1175/JCLI4056.1, 2007.
- 1314 Yu, H. B., Chin, M., Bian, H. S., Yuan, T. L., Prospero, J. M., Omar, A. H., Remer, L. A., Winker, D. M., Yang, Y. K.,
1315 Zhang, Y., and Zhang, Z. B.: Quantification of trans-Atlantic dust transport from seven-year (2007-2013) record of
1316 CALIPSO lidar measurements, *Remote Sens Environ*, 159, 232-249, 10.1016/j.rse.2014.12.010, 2015.

1317 Zobeck, T. M., Sterk, G., Funk, R., Rajot, J. L., Stout, J. E., and Van Pelt, R. S.: Measurement and data analysis methods for
1318 field-scale wind erosion studies and model validation, *Earth Surface Processes and Landforms*, 28, 1163-1188,
1319 10.1002/esp.1033, 2003.

1320